Frequency stabilization of a Titanium-Sapphire laser for precision spectroscopy on Calcium ions

Gerhard Kirchmair

Contents

Abstract

This thesis reports on the stabilization of a Titanium-Sapphire laser onto a high finesse cavity for precision spectroscopy on $^{40}Ca^+$ and $^{43}Ca^+$.

The setup of the laser and the optics, as well as the setup of the high finesse cavity will be discussed. Important cornerstones are explained to get a laser linewidth in the few Hz regime. The linewidth of the laser is estimated from the error signal and determined by a beat measurement with a similar laser.

Additionally, results on the spectroscopy of $^{40}Ca^+$ in a linear Paul trap are presented in the last chapter.

Introduction

High precision spectroscopy with single trapped ions and the ability to manipulate ions individually, set the stage for recent experiments on quantum information [1, 2] and optical clocks [3]. Especially the development of narrowband lasers [4, 5] has opened a door for many high precision measurements.

In spectroscopy widely tunable solid state lasers provide the experimentalist with a versatile tool, as any atomic or molecular resonance can be excited within a broad frequency range. At the same time a small linewidth may be necessary to resolve, for example, forbidden transitions. So far laser frequency stability has been demonstrated at a level of 10^{-15} in 32 s for two independent systems [4]. This impressive performance is achieved by applying a continuous correction to the laser derived from a sensitive frequency discriminator. Often a high finesse cavity is used for this purpose. The basic methods for laser stabilization onto a cavity were invented in the eightiess by J. L. Hall [6], [7] and others and were refined over the years. Cavities made of ultra low expansion material (ULE) with special designs for low acceleration sensitivity and narrow resonances, are the basis of todays ultra stable lasers. These cavities are the flywheel in the new optical clock generation which is currently developed.

Another application for very stable lasers is the field of quantum information processing with ions in radio frequency traps. In the last couple of years several experiments [1, 2] were performed, which are first steps towards a functioning quantum computer. These experiments rely on experimental techniques which require narrowband lasers. Examples for these techniques are cooling to the ground state, state preparation, efficient detection and state manipulation. One approach pioneered in Innsbruck, is the use of a forbidden transition for manipulating quantum information by coherent laser light. These transitions have a typical linewidth around 1 Hz. A laser manipulating this transition must be as narrowband as possible in order to obtain long coherence times and get low error rates.

Research projects within our group focus on quantum information processing and precision spectroscopy with ions stored in radio frequency traps. In one experiment a string of $^{40}Ca^+$ ions stored in a linear Paul trap, is used to perform quantum algorithms and investigate multiparticle entanglement. Microtraps are developed to improve the scalability of ion trap quantum computers. Quantum computation techniques are investigated to improve frequency metrology which might be used in optical frequency standards. Five experiments are located at the Institute for Experimental Physics of the University of Innsbruck including an ultra stable Titanium Sapphire laser ($^{40}Ca^+$ TiSa). Two experiments are

situated at the "Institut für Quantenoptik und Quanteninformation" (IQOQI) of the Austrian academy of sciences. One of these experiments is focused on quantum information processing with $^{43}Ca^+$ and $^{40}Ca^+$ in a linear Paul trap. This thesis reports on the construction of an ultra stable Titanium Sapphire laser ($^{43}Ca^+$ TiSa) for the experiments based on $^{43}Ca^+$ ions.

The two buildings are connected via a bundle of 500 m long optical fibers[1]. This link is used for comparing ultrastable lasers and allows us to send light to the frequency comb in the university building. This link will be used in the future to connect two experiments.

In this work the necessary steps to built a Titanium Sapphire laser with a few Hz linewidth are discussed. A short outline of the purpose of the laser will be given in the first chapter. The second chapter explains the setup of the laser. Chapter three and four present the optical and cavity setup. Temperature stabilization and vibration isolation are discussed. Chapter five shows the basics of feedback, the derivation of the Pound-Drever-Hall locking signal and the actual stabilization of the laser. In chapter six the linewidth of the laser is determined and chapter seven shows results on the spectroscopy of $^{40}Ca^+$ done with this laser. The appendix concludes the work with the necessary circuits and a short explanation of them.

---

[1]Laser 2000: 2 x standard single mode, 2 x single mode 780-970 nm, 1 x single mode 600-760 nm, 1 x PM - fiber 800-980 nm, 1 x PM - fiber 630 - 780 nm.

Chapter 1

Quantum information processing

Quantum computers have the potential to efficiently solve problems which are practically impossible for classical computers. Examples are the factorization of large numbers into primes and the simulation of quantum systems. This is achieved by exploiting the laws of quantum mechanics that allow to perform computation with superpositions of quantum states.

In a quantum computer, a quantum bit (qubit) represents the basic unit of computation. A qubit is encoded in two orthogonal quantum states. Any superposition of these two states is an allowed state of the qubit.

Over the last years several candidates for qubits have been investigated. Some of the most promising results, like teleportation [2], quantum error correction [9], states of six/eight entangled qubits [8]/[1], were shown with ions stored in a radio frequency (RF) trap. Other possible systems are solid state qubits [10], neutral atoms[11] and NMR [12].

A quantum computation can be divided in the following steps:

1. State initialization.

2. Execution of quantum algorithms on the qubits. It can be shown, that every possible quantum algorithm can be performed with single qubit rotations and universal two qubit gates [13].

3. Quantum state measurerement. The result of the computation is read out by projecting the qubits onto their basis states.

In this chapter a very brief summary will be given on ion trap quantum computation. For a more detailed overview papers by A. Steane [15] and D. F. V. James [14] and the references in there are recommended. The purpose of the 729 nm laser for the Innsbruck quantum information experiment based on $^{43}Ca^+$ will be outlined.

1

1.1   Ingredients for an ion string quantum computer

The first proposal for a quantum computer based on an ion string, was published by Cirac & Zoller [16] in 1995. There they suggested the use of two internal states of an ion as a qubit. The harmonic motion of the ion string in the trap is used for transferring quantum information between the qubits and for realizing quantum gates. The combination of the qubit states and motional states of the harmonic oscillator results in a ladder like scheme which is shown in Figure 1.1.
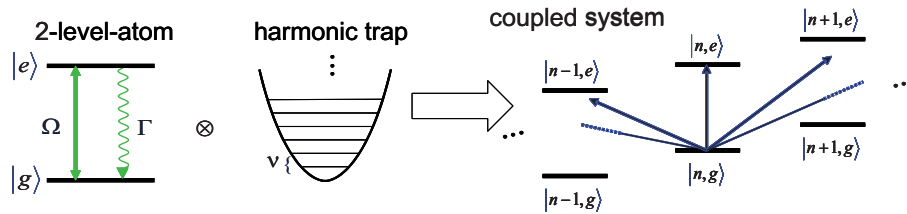
Figure 1.1: Internal levels and motional states of an ion in a harmonic potential (n is the quantum number of the harmonic oscillator)

The initial state of the qubit is prepared by Doppler-cooling and sideband cooling the ions to their motional ground state and by optical pumping that populates a single internal state of the ion. This can be done with an efficiency of more than 99 % [18].

Single qubit gates can be performed by manipulating the internal state of the ion. Two qubit gates are obtained with the help of the common motion [16], where a laser for example couples the states $|n, g>$ and $|n + 1, e>$ mapping thereby the internal state of the ion to the motional state. The motion of the ions serves therefore as a bus system with which two-qubit gates can be performed. Transitions that only change the electronic state of the ion are called *carrier transitions*. Transitions that also change the motional state of the ion string are called sideband transitions. *Blue sideband* transitions increase the motional quantum number by one where as *red sideband* transitions decrease it by one whenever the ion is excited to the upper level.

Finally, a selective read-out of the state of the ions is required which is accomplished by electron shelving [17]. The ion is repeatedly excited on a transition that couples the electronic ground state to a short lived (about 10 ns) excited state. A schematic level scheme for electron shelving is shown in Figure 1.2. On a closed cycle an ion can scatter a lot of photons per second and if only one of the two qubit levels ($|0>, |1>$) couples to the exciting laser the state of the ion can be detected by measuring the fluorescence.

1.2   Ion species

So far the quantum information experiment in our group used $^{40}Ca^+$ as a qubit. The level scheme is shown in Figure 1.3. The qubit consists of the $S_{1/2}$ and
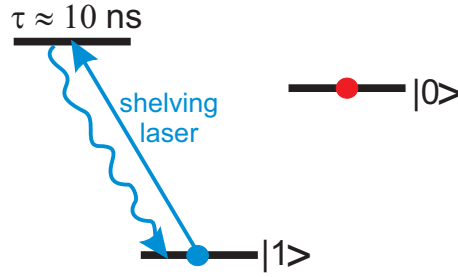
Figure 1.2: Electron shelving. The qubit consisting of the $|0>$ and $|1>$ levels is state selectively read out with a shelving laser resonant to a level with a short lifetime. Only the $|1>$ state couples to the laser light. From the excited state it quickly (about 10 ns) decays back to the ground state by emitting a photon. The electron gets repeatedly excited and scatters a lot of photons per second which can be detected by a camera or photomultiplier.

the $D_{5/2}$ level. This choice is suitable as qubit due to the long lifetime of the $D_{5/2}$ level which is about 1 s. A 729 nm laser with narrow linewidth is able to coherently transfer population between the $S_{1/2}$ and the $D_{5/2}$ level.

The 397 nm laser is used for Doppler cooling and electron shelving on the $S_{1/2}$ to $P_{1/2}$ transition. A repumping laser at 866 nm is necessary to prevent population transfer into the $D_{3/2}$ level.
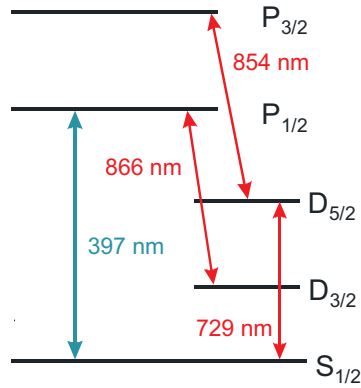
Figure 1.3: Level structure of $^{40}Ca^+$. The qubit consists of the $S_{1/2}$ and the $D_{5/2}$ levels which are coupled by a 729 nm laser. The lifetime of the $D_{5/2}$ level is about 1 s. The 397 nm laser is used for Doppler cooling and electron shelving. The 866 nm laser repumps the ion from the $D_{3/2}$ level. The 854 nm laser is used for repumping and sideband cooling purposes.

Experiments utilizing the quadrupole transition from the $S_{1/2}$ to the $D_{5/2}$ state for quantum state manipulation are effected by two sources of decoherence:

- A finite laser linewidth will lead to a dephasing of the electric field with respect to the atomic superposition states phase.

- Magnetic field fluctuations will similarly lead to a dephasing by changing the atomic transition frequency via the first order Zeeman effect.

Currently, both effects limit the coherence time in the experiment to roughly 3 ms.

To get rid of these effects a new experiment has been set up. Here $^{43}Ca^+$ which has a nuclear spin of 7/2 will be used as the qubit ion. The qubit will be encoded in two hyperfine states of the $S_{1/2}$. Quantum information will be manipulated by driving Raman transitions between the qubit-states using a laser at 395 nm. This scheme has the following advantages:

- Quantum information can be encoded in states that are magnetic field insensitive. At low magnetic fields the states $S_{1/2}$, F = 4, m_f = 0 to $S_{1/2}$, F = 3, m_f = 0 possess this property.

- For the Raman transition only the difference frequency of the two laser beams has to be stable. The Raman beams can be produced from a single laser beam by shifting its frequency using acousto-optical modulators (AOM). The AOMs are driven by RF sources which are connected to a 10 MHz reference.

- Due to the similarity of $^{43}Ca^+$ with $^{40}Ca^+$, basically the same laser system can be used for both isotopes.

The level scheme for $^{43}Ca^+$ shown in Figure 1.4 is a little bit more complicated due to the additional fine structure splitting.

The setup of the 729 nm laser has to be designed in such a way that the laser can be tuned to any transition frequency from $S_{1/2}$ to $D_{5/2}$ for both Ca^+ isotopes. This already sets several requirements:

- The laser has to be tunable by 100 MHz to cover the hyperfine splitting of the $^{43}Ca^+$ $D_{5/2}$ level. Some experiments require the consecutive manipulation of different transitions in a few μs. Thus a change of the frequency has to be possible within few μs.

- The isotope shift between $^{43}Ca^+$ and $^{40}Ca^+$ is on the order of 4.1 GHz [19]. Additionally the hyperfine splitting of the $S_{1/2}$ of 3.2 GHz has to be taken into account. Thus it must be possible to change the frequency of the laser by 5.5 GHz.

1.3   Purpose of the 729 nm laser

In experiments with $^{40}Ca^+$ or $^{43}Ca^+$ the 729 nm laser can be used for:

1. preparing an ion in the motional ground state by sideband cooling

2. measuring the strength of the magnetic field by spectroscopy on the quadrupole transition
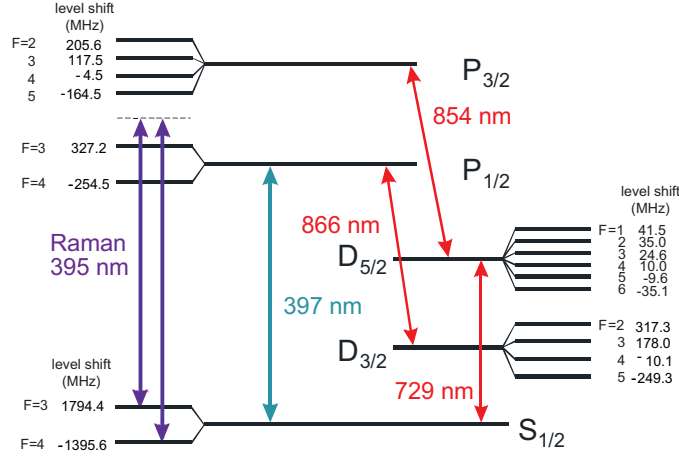
Figure 1.4: Level structure of $^{43}Ca^+$. The qubit consists of the $S_{1/2}$, F = 4, $m_f = 0$ and $S_{1/2}$, F = 3, $m_f = 0$ levels. The transition is driven with a 395 nm Raman laser. The purpose of the other lasers is the same as for the $^{40}Ca^+$ experiment. The numbers next to the levels denote the hyperfine state and the level shift relative to the line center due to the hyperfine splitting.

3. micromotion compensation

In addition the laser will be used for qubit state detection in the $^{43}Ca^+$ experiment.

1.3.1 Sideband cooling in $^{40}Ca^+$

When ions are trapped in an ion trap, they typically have temperatures of several hundred to thousand K unless they are cooled by lasers. The first cooling step with $^{40}Ca^+$ ions is Doppler cooling with a 397 nm laser on the $S_{1/2}$ to $P_{1/2}$ transition. For a trap frequency of about 1 MHz the Doppler cooling limit results in an average vibrational quantum number of about 10 [18]. Thus a second cooling step is required to get to the motional ground state. This can be done by sideband cooling the ions with a 729 nm laser on the $S_{1/2}$ to $D_{5/2}$ transition.

If the laser is tuned to the red sideband transition, the ion is transferred to the $D_{5/2}$ level and simultaneously the motional quantum number n is reduced by one. The natural lifetime of this level is about one second, so for efficient cooling the $D_{5/2}$ level needs to be coupled to the fast decaying $P_{3/2}$ by a 854 nm laser. From the $P_{3/2}$ level it decays back into the $S_{1/2}$ by spontaneously emitting a photon. In this simple description the possibility of the ion decaying into the $D_{3/2}$ instead of the $S_{1/2}$ level has been neglected. If this happens the ion is repumped by the 866 nm laser but now a decay into the wrong $S_{1/2}$ state is possible and the cycle is not closed. Short σ^+ or σ^- polarized 397 nm
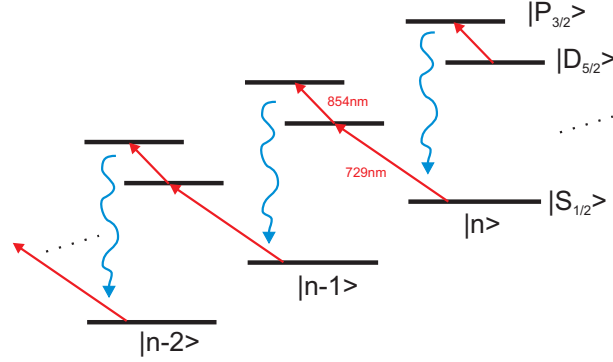
Figure 1.5: Sideband cooling in $^{40}Ca^+$. A 729 nm laser transfers the ion from the $S_{1/2}$ to the $D_{5/2}$ state thereby reducing the motional quantum number n by one. A 854 nm laser then transfers the ion to the $P_{3/2}$. From there it quickly decays back into the ground state by emitting a photon. This cycle is repeated until the ion is in the ground state.

light pulses, depending on the ground state used, counter this and bring the population back into the cycle.

For an effective cooling the trap frequency has to be large compared to the decay rate of the excited state and the laser linewidth [18]. The cooling rate depends on the power of the 729 nm laser. Optimal cooling results have been achieved with a Rabi frequency of 50 kHz [18]. This value already limits the laser linewidth that has to be achieved to around 1 kHz. For bigger linewidth the cooling becomes less efficient [20].

1.3.2 Spectroscopy of the $S_{1/2}$ to $D_{5/2}$ transition of Ca^+

With the help of a 729.147 nm laser the $S_{1/2}$ to $D_{5/2}$ transition frequencies can be determined. The degeneracy of the states is lifted by an external magnetic field. Due to the Zeeman splitting several different spectral lines can be seen. Additionally, every line acquires sidebands due to the harmonic trapping potential and micromotion (see chapter 1.3.3). The frequency of the sidebands created by the trapping potential depend on the strength of the confinement [21]. The spectra can be recorded by exciting the transition and measuring the occupation probability of the $S_{1/2}$ state with the 397 nm laser. The resolution of the spectrum is limited by different factors:

- The natural linewidth of the transition of 0.16 Hz

- Laser frequency fluctuations

- Magnetic field fluctuations

If one wants to resolve the natural linewidth a laser stability below 0.16 Hz is necessary. This leads to the strongest constraints regarding the linewidth of the laser. For a first step, the aim is to achieve a laser linewidth below 10 Hz.

Magnetic field fluctuations can be eliminated by using magnetic field insensitive transitions, which are available in $^{43}Ca^+$. A possible candidate is the m_f = 0 to m_f = 0 at a low magnetic field. Another example is the $S_{1/2}$, F = 4, m_f = 4 to $D_{5/2}$, F = 4 m_f = 3 transition at a magnetic field of 3.4 Gauss. These transitions might be used as an optical frequency reference.

1.3.3 Micromotion compensation

Stray electric fields move the ion out of the center of the trap. Under the influence of the driving RF field it will oscillate. The motion of the ion leads to a Doppler shift and thus to changing atomic transition frequencies. A narrow transition (e.g. quadrupole transition in $^{40}Ca^+$) acquires sidebands at the frequency of the ion motion where as dipole transitions get broadened. This broadening reduces the efficiency of laser cooling and thus has to be canceled. By applying DC voltages to compensation electrodes, these stray electric fields can be countered and the ion is moved back into the trap center.

A coarse compensation in two dimensions can be achieved by looking at the CCD image of the ion. The ion has to be moved to a point where its position is independent of the power of the driving RF field. This method only works at low trap frequencies and allows no compensation along the CCD axis.

Another experimental technique is to measure the Rabi frequency of the micro-motional sidebands of one of the $S_{1/2}$ to $D_{5/2}$ transitions. The strength of this sideband compared to the carrier is a direct measure of the modulation index. If the ion is far out of the center of the trap many sidebands can be detected. By applying a DC voltage to the compensation electrodes the number and strength of these sidebands can be reduced. The value of the compensation voltages can be chosen such that the modulation index is minimal and only weak sidebands occur. With 729 nm beams coming from different directions a compensation of the motion in all axes is possible [18].

1.3.4 State detection in $^{43}Ca^+$

Both qubit levels in $^{43}Ca^+$ couple to a 397 nm shelving laser. Thus the read out scheme has to be modified (Figure 1.6). The 729 nm laser transfers one of the two qubit populations adiabatically to the $D_{5/2}$ level. The population of the other state is unaffected by the adiabatic passage and can be read out by the standard electron shelving technique with a 397 nm laser.

1.4 Specifications of the 729 nm laser

In summary the 729 nm laser needs to fulfill the following requirements:

- A frequency change of the laser by 100 MHz on the μs timescale has to be possible.

- The 5.5 GHz frequency gap between $^{40}Ca^+$ and $^{43}Ca^+$ has to be bridged.
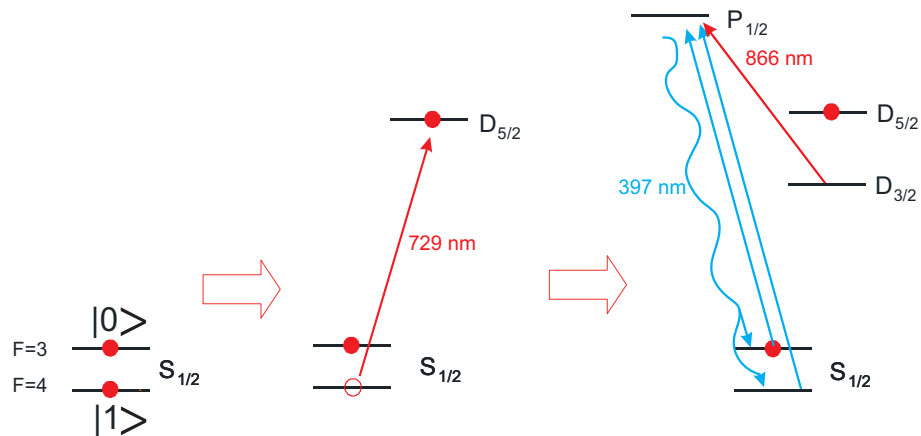
Figure 1.6: State detection with $^{43}Ca^+$. The population of one of the qubit states is transfered to the $D_{5/2}$ level. The population of the other state is unaffected and can be read out by the 397 nm shelving laser. The 866 nm laser is used for repumping the ion from the $D_{3/2}$ level.

- The lock of the laser to the cavity should be stable for several hours.

- A laser linewidth of 10 Hz.

- The drift of the laser-frequency should be below 1 Hz/s.

Chapter 2

The Titanium Sapphire laser

To generate light of 729 nm, a Coherent 899 Titanium Sapphire (TiSa) ring laser is used. It is pumped by a solid state diode pumped Nd:YVO$_4$ laser at 532 nm[1]. The TiSa laser provides high power and in its original configuration a linewidth of roughly 500 kHz. The standard 899 ring laser was upgraded by intracavity elements and an additional EOM. In the following chapters the general mode of operation of the TiSa laser will be described, followed by the explanation of the setup and purpose of the intracavity elements.

2.1 Mode of operation of a TiSa laser

As active medium solid state lasers use metal ions embedded in a transparent crystal. In the case of a TiSa laser it is a Ti^{3+} ion which is doped into sapphire, Al$_2$O$_3$, as host. This small amount of Titanium (roughly 0.1%) is then responsible for the lasing emission.

Figure 2.1 shows the 3d^1 absorption and emission band of the Ti^{3+} ion. The surrounding crystal field splits this level up into the ^{2}T$_{2g}$ and the ^{2}E$_g$ levels. These levels get split further by the spin orbit interaction and experience a big broadening. This broadening is caused by the interaction of the ion with lattice vibrations.
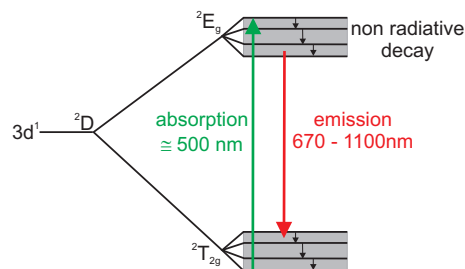
Figure 2.1: Level scheme of the Ti^{3+} ion in sapphire. The splitting is due to the crystal field while the broadening of the lines results from spin orbit interactions and lattice vibrations.

---

[1]Coherent, Verdi V10

Population inversion is achieved by a strong pump laser populating a high vibrational mode of the ^2E_g level. The electrons then decay very quickly by phonon interaction into a lower vibrational mode. A decay by emission of a photon into a vibrational mode of the $^2T_{2g}$ level is followed by a non-radiative decay into the ground state [22]. This effectively corresponds to a four level laser where two transitions occur by a fast non-radiative decay. Because of these non-radiative decays, the emission spectrum of the TiSa is as broad as 600 nm. The laser is able to emit on all lines where the gain of the medium exceeds the losses. To avoid multimode lasing, additional frequency selective elements inside the laser help to select a single mode.

A further advantage of the TiSa crystal is the very good mechanical stability and the high heat conductivity which renders it pretty stable in frequency and power output.

2.2   Intracavity elements of the TiSa laser

Figure 2.2 shows the setup of the Coherent 899 TiSa ring laser. The ring cavity consists of four mirrors, the TiSa crystal as a gain medium, as well as a birefringent filer, an optical diode, a Brewster plate, a thick and a thin etalon. The purpose of the EOM in the beam path will be explained in chapter 5.3.
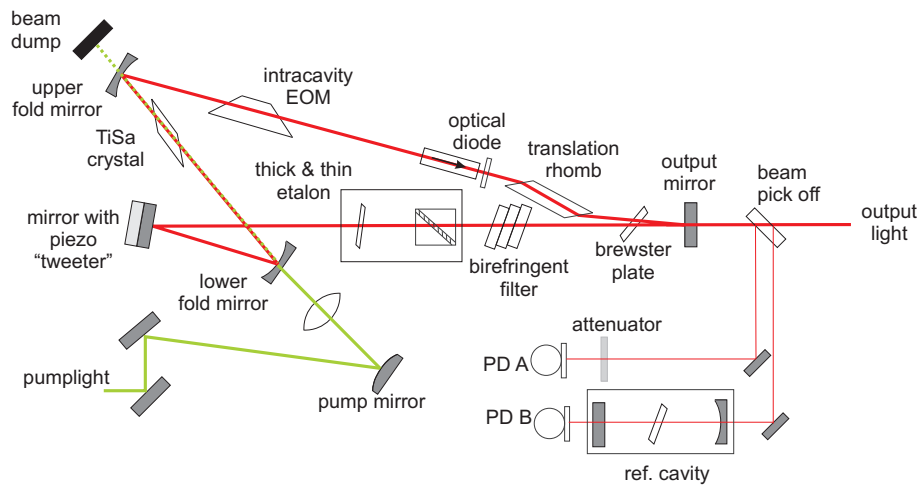
Figure 2.2: Optical setup of the TiSa laser.

The laser was set up according to the Coherent operator's manual. Hints regarding the operation of the laser are given in chapter A.2.

In TiSa lasers the gain profile of the active medium is very broad, and many eigenmodes of the laser cavity get amplified and can participate in the laser oscillation. For spectroscopy the laser output should be single mode, so the laser has to be built in such a way that this is achieved. The laser cavity has a geometry such that higher transverse modes are already suppressed and single transverse mode operation is achieved [24]. Nevertheless, the laser can still

oscillate on several different longitudinal modes which have to be eliminated. This is obtained by adding some elements inside the laser cavity.

2.2.1 Birefringent filter

The first element discussed here is the birefringent filter. It consists of three birefringent plates with a thickness ratio of 1:4:16. Light that is traveling through one of these plates gets split up in an ordinary and extraordinary ray, which propagate at different speeds trough the plate. This leads to a rotation of polarization equal to

$$\Delta\Phi = 2\pi \frac{l}{\lambda} \Delta n, \tag{2.1}$$

where l is the thickness of the plate and Δn the difference in the refractive index for ordinary and extraordinary ray. Only wavelengths at which these two rays have optical path lengths equal to an integer multiple of the wavelength don't get rotated. The exit facet of the plate is at Brewster angle and light which is rotated experiences higher losses, so that a filter with a transmission equal to

$$T(\lambda) = \cos^2(\frac{2\pi}{\lambda} l \,\Delta n) + T_s \sin^2(\frac{2\pi}{\lambda} l \,\Delta n) \tag{2.2}$$

results, where T_s is the transmission coefficient of the s-polarized part of the light at Brewster angle. In the laser three plates are used to triple the losses of the rotated light to get a narrow filter with the desired mode spacing. The tuning of the filter is done by slightly changing the angle of the plates. Thus the effective length changes and with it the frequency of the transmission peak. This already limits the possible laser frequencies. Still further elements are needed to achieve single mode operation.

2.2.2 Thick and thin etalon

By inserting a tilted glass plate with thickness t and refractive index n into the laser cavity a further mode filtering can be achieved. This etalon has transmission maxima at wavelength λ_m [24] with

$$m\lambda_m = 2nt \cos\theta \tag{2.3}$$

where m is an integer number and θ the angle between light and normal on the plate. The transmission function has a comb structure and the wavelengths of the maxima are set by the angle and the thickness of the plate. Since the wavelength is also set by the resonator cavity, one has to ensure that the transmission peak of the etalon coincides with an eigenmode of the resonator satisfying the condition

$$m\lambda_m = 2n\,t\,\cos\theta = \frac{d}{q} \rightarrow \cos\theta = \frac{m}{2q}\frac{d}{n\,t}. \tag{2.4}$$

Here, d is the length of the ring resonator and q an integer number. Normally, the free spectral range (FSR) of the etalon

$$FSR = c\,\frac{m+1}{\lambda_m} \tag{2.5}$$

is larger than the spectral width of the combined gain profile of gain medium and resonator mirrors, which guarantees that only one mode lies above the lasing threshold. Due to the broad gain profile of the TiSa laser one etalon is not sufficient and therefore a second etalon with different thickness is added into the beam path.

Two Littrow prisms on piezoelectric translators form the thick etalon. This configuration is equivalent to a glassplate, but has the advantage of a tunable thickness. The second thin etalon is a galvo controlled glass plate where the angle is tuned. This results in two differently spaced combs which have to be overlapped on one frequency, to get a transmission maximum.
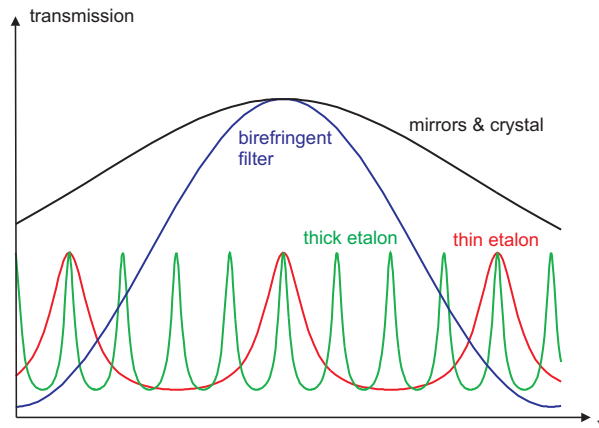
Figure 2.3: Transmission curves for the different intracavity parts. For a single mode operation the transmission maxima of the different elements have to coincide in one point.

In Figure 2.3 a schematic picture of the different transmission profiles of the frequency selective parts can be seen. All curves have to coincide in the point where the lasing should occur. If one of the elements is not in the right position the laser will either not lase or run multimode. By adding them all up (multiplying the transmission functions) one obtains the overall transmission profile (see Figure 2.4) of the intracavity elements.

Also depicted in Figure 2.4 is the threshold above which lasing can occur. This threshold arises from the losses generated by the elements in the cavity. One can see that all modes except the one right in the middle of the central peak get suppressed and single mode operation is achieved.

2.2.3   Optical diode

Laser light in the TiSa is emitted by the crystal in both directions, yielding a standing wave inside the ring resonator. Standing waves lead to spatial hole burning in the active medium. Here spatial hole burning means that in the nodes of the standing wave, the population inversion created by the pump laser,
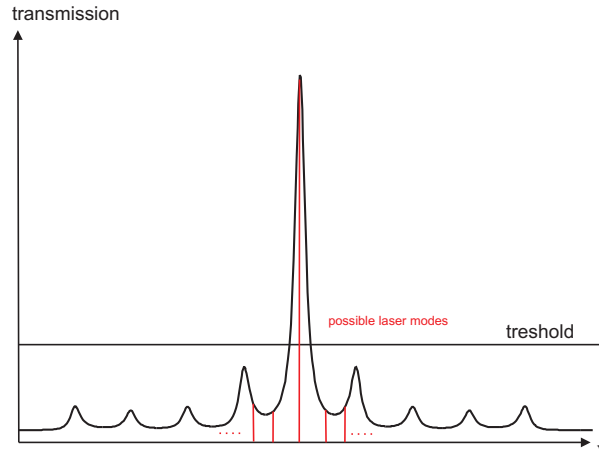
Figure 2.4: Combined transmission profile of the intracavity parts. Only one mode is above the lasing threshold, thus single mode operation is achieved.

can't be utilized and doesn't contribute to the laser emission. But a different mode shifted by $\lambda/4$ can use this population inversion and might have enough gain to grow. This would result in a mode competition between two modes and give rise to oscillations and spikes in the output power.
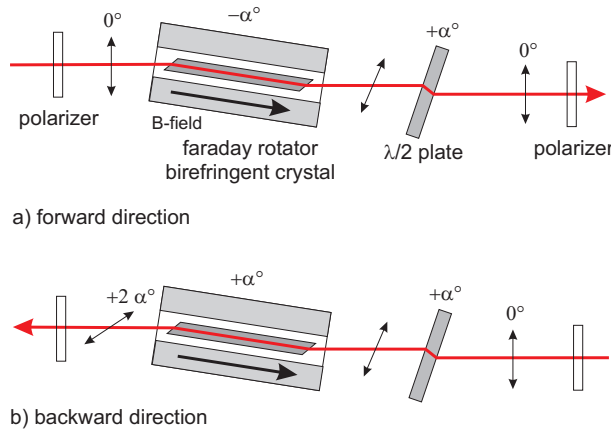
Figure 2.5: Rotation of the polarization inside an optical diode for waves in a) forward and b) backward direction [24]. Light propagating in the backward direction experiences higher losses and is suppressed.

To avoid a propagation of laser waves in both directions an optical diode is placed inside the ring resonator. An optical diode consists of a Faraday rotator, a $\lambda/2$ plate and elements with a polarization dependent transmission, like Brewster windows or polarizers. Figure 2.5 shows how an optical diode works [24]. The polarization of the wave traveling in forward direction is rotated in the $\lambda/2$ plate by $\alpha°$ and in the Faraday rotator by $-\alpha°$, so that no net polarization rotation occurs. Light traveling in the other direction gets rotated by $2 \cdot \alpha°$ which causes losses. α is typically in the order of $3°$ for the optical diodes

used inside the TiSa. This symmetry breaking is caused by a magnetic field applied along the axes of the birefringent crystal inside the Faraday rotator. If the losses are large enough for light travelling in one direction it can't reach the threshold necessary for lasing.

After inserting the optical diode the laser field is a traveling wave which can use the total population inversion. One therefore gets a more stable and even larger power output.

2.3 Coherent locking scheme

An electronic box is supplied with the laser which provides feedback on the laser for narrowing the linewidth and allows a 30 GHz mode-hop-free scanning. In this section the different servo loops in the box and the changes made to improve the system, will be explained.

Figure 2.6: Schematical overview of the locking circuits of the Coherent control box. Blocks shaded in gray are elements inside the TiSa. The different blocks are explained in chapters 2.3.1 and 2.3.2.

In Figure 2.6 all of the important elements for the Coherent lock of the TiSa are shown. The circuit paths are color coded to display the different locking modes of the system. The parts added to improve and adjust the system are shown in green and will be explained in the following. The purpose of the different system blocks will be explained in chapter 2.3.1 and 2.3.2.

2.3.1 Thick etalon lock

The thick etalon is very sensitive to temperature changes which change the distance between the two Littrow prisms. To compensate for that, the thick etalon prisms are mounted on a piezoelectric translator to control the distance.

The distance of the prisms is wiggled by a small amount with a 2 kHz sine wave applied to the piezo, which causes amplitude fluctuations at a frequency of 2 kHz in the output light. These fluctuations are detected by the reference photodiode PD A shown in Figure 2.6 and 2.2. The detected signal is multiplied on one hand with the squared 2 kHz sine and on the other hand with the squared and inverted sine. The resulting two signals are then subtracted from each other and subsequently integrated. This is a so called lock-in-detection. The different stages are shown in the thick etalon block in Figure 2.6. In Φ-det happens the multiplication, subtraction and integration of the signals. If the thick etalon is in the transmission maximum of the other intracavity elements there is a phase difference of 90° between the original drive signal and the oscillation detected by the photodiode. This then yields a zero voltage at the output of Φ-det. If the etalon drifts off the transmission maximum, the phase difference between the applied 2 kHz signal and the detected signal changes. A positive or negative voltage is created at the output of Φ-det, depending on the length increase or decrease of the etalon. This voltage is then fed back on the piezo to bring the etalon back to the right position.

The 2 kHz jitter of the etalon also causes frequency fluctuations. To compensate for that a circuit is added. This circuit is not supplied with the box and was built by us (see appendix B.3). The signal of the oscillator is phase shifted and attenuated and then applied to the piezo of a mirror inside the TiSa. This mirror is called tweeter (see Figure 2.2). With this feed forward the length of the ring cavity is kept constant and the frequency fluctuations vanish. Since the internal 2 kHz oscillator produces higher harmonics, which cause similar problems, it was replaced by an external function generator (see Figure 2.6). The 2 kHz modulation can also be seen in the amplitude spectrum of the light. An external intensity stabilization is used to suppress this modulation and other perturbations of the amplitude (see Chapter 4.2 & Figure 2.9). The changes made in the Coherent lock box can be found in appendix A.1.

2.3.2 Linewidth reduction

The laser frequency varies due to changes in the cavity length, caused by thermal effects and vibrations. A feedback is required to get the linewidth to 500 kHz.

Photodiode (PD) B (see Figure 2.6) detects the laserlight transmitted through the low finesse reference cavity. In the differential amplifier this signal is added to the constant negative signal of PD A which monitors the light intensity of the laser. By setting the signal of PD A to half the peak voltage of the cavity transmission one creates a locking point at half the hight of the cavity fringes independent of the output power of the laser. The different signals and the lock position is shown in Figure 2.7.
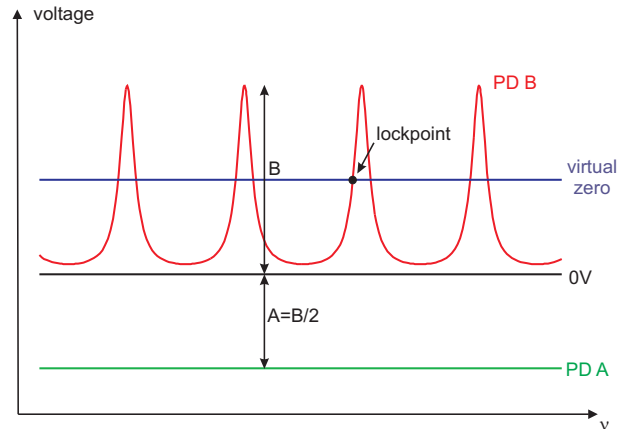
Figure 2.7: Signals of the side of fringe lock. The light power detected by photodiode A is subtracted from the transmission signal of the reference cavity detected by phodiode B. This shifts the cavity transmission signal and creates a lock point at the side of the fringe.

The feedback is applied to the piezo of the tweeter mirror and the scanning Brewster plate, which can change its angle and therefore the effective length. The scanning Brewster plate has a frequency response of 400 Hz and a correction range of 15 GHz. It is responsible for correcting the slow drifts of the laser cavity. The tweeter's lowest eigenfrequency is 6 kHz (depending on the piezos used) and has a correction range of 1 GHz. By the use of a "tweeter trap" (filter), one can achieve an in phase frequency response of up to 10 kHz, to compensate distortions such as acoustics. With this feedback scheme the linewidth is reduced to about 500 kHz.

The lockbox is also capable of scanning the laser over 30 GHz by scanning a galvo plate inside the reference cavity to which the laser is locked. The signal used for scanning the cavity is fed forward to most of the elements. This roughly positions the elements so that the servo can take over and lock it to the scanning cavity.

2.3.3   Amplitude noise spectra of TiSa and Verdi

There are amplitude fluctuations in the output power of the TiSa. Some of these fluctuations are correlated with amplitude noise in the pump laser[2], others are produced within the TiSa.

As can be seen in Figure 2.8, fluctuations of the pump light cause fluctuations in the output light of the TiSa at exactly the same frequency. The peaks that dominate the TiSa spectrum are at 109.3 kHz and 218.6 kHz and correspond to power fluctuations of about 0.03 %. The magnitude of the TiSa fluctuations can not be explained by considering only the amplitude fluctuations of the pump laser. A possible explanation could be beam steering of the pump laser with the
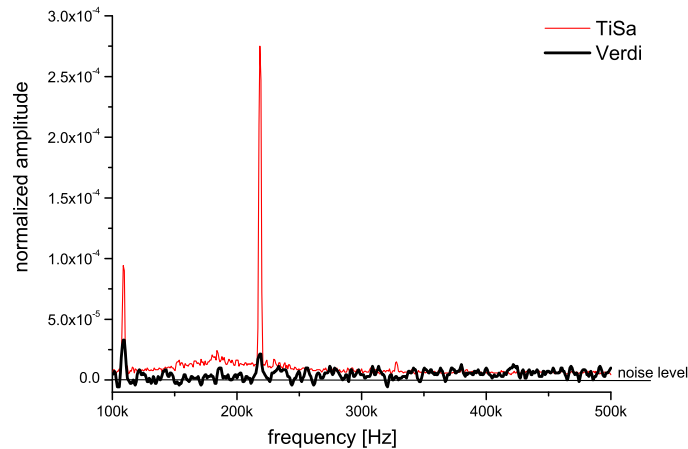
---

[2]Coherent Verdi V10

Figure 2.8: Comparison of the amplitude noise spectra of the TiSa and the Verdi pump laser. The amplitude of the fluctuations was normalized to the DC light power. The peaks dominating the spectra are at 109.3 kHz and 218.6 kHz for Verdi and TiSa. The magnitude of these peaks should not be a problem for the experiment.

same frequencies. This could create additional oscillations inside the TiSa but this issue has not been investigated. The intensity fluctuations for the pump laser are well within the specifications, below 10^{-4}, and the fluctuations in the TiSa are small enough that they should not harm the experiment. The spectra were recorded by placing a photoreceiver[3] in the attenuated output beam of the TiSa or the attenuated pump laser light. The measurement was done for frequencies up to 5 MHz, but above 500 kHz the spectrum of both lasers is completely flat. In Figure 2.8 the spectra were normalized to the DC light intensities. The resolution bandwidth of the spectrum analyzer[4] used for this measurement was 1 kHz.

Spectra were also recorded in the range from DC to 100 kHz but no fluctuations were found in the pump light. For the TiSa though, there are some unwanted features. Plotted in Figure 2.9 is the amplitude noise spectrum of the TiSa in the range from 0 to 6 kHz (measurements were done up to 100 kHz).

In Figure 2.9 one can clearly see 2 kHz and 4 kHz fluctuations which are caused by the thick etalon lock and low frequency noise caused by acoustics in the lab. A photodiode[5] and a FFT analyzer[6] working with a resolution bandwidth of 16 Hz were used to record the spectra. The amplitude of the signal was again normalized with the DC amplitude of the light. In addition Figure 2.9 shows the effect of the intensity stabilization, which reduces the noise

---

[3]New Focus, model 1801-FS Si 125-MHz
[4]Rohde & Schwarz FSP Spectrum Analyzer 9 KHz - 13.6 GHz
[5]Thorlabs PDA 520
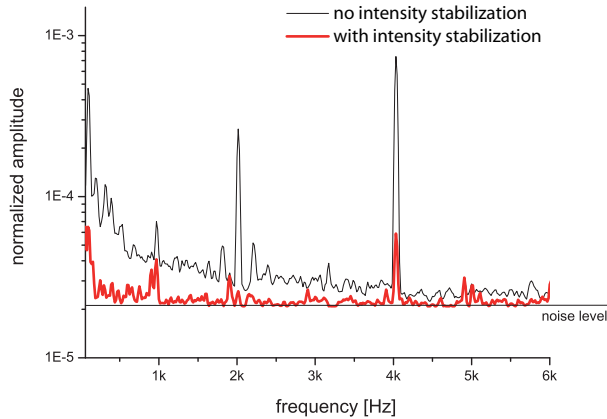[6]SRS SR 760 FFT spectrum analyzer

Figure 2.9: TiSa amplitude noise spectrum with and without intensity stabilization. Peaks at 2 kHz and 4 kHz dominate the spectrum. They are produced by the electronics of the thick etalon lock. The intensity stabilization reduces them by an order of magnitude.

by an order of magnitude below 20 kHz. The highest peak in the unregulated signal corresponds to an amplitude fluctuation of around 0.1 % and gets reduced to below 0.01 %. Much bigger amplitude variations, on the order of 5-10 % occur at a timescale of minutes and hours due to temperature changes in the TiSa. These can also be compensated with the servo (see chapter 4.2).

2.3.4   Output vs. pump power

Figure 2.10 shows the dependence of the output power of the TiSa on the pump power. This is a typical plot, but the output power of the TiSa can vary from day to day by up to 10 %. The highest output power was 600 mW for a pump power of 6.5W. Usually the output is around 500 mW. The lasing threshold typically lies around 4.5 W but the TiSa output power is more stable for pump powers above 6 W.

During the operation of the laser, the piezo adjusting the thick etalon broke and a new one had to be build in. With this etalon the output power dropped by 10 % to about 450 mW for a 6.5 W pump power.
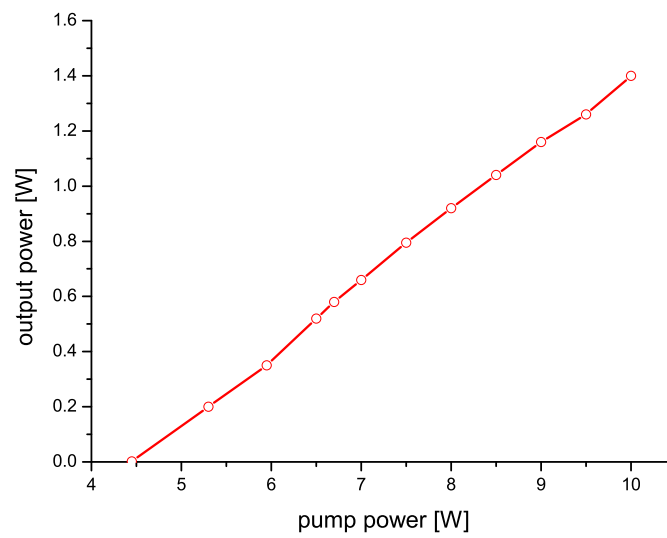
Figure 2.10: Output power of the TiSa vs. pump power. The lasing threshold lies around 4.5 W pump power.

Chapter 3

High finesse cavity

To achieve a narrow band laser a stable reference for locking the laser frequency is needed. The most stable lasers have recently been built with the help of high finesse cavities [4]. The cavity serves as a frequency discriminator which makes it possible to stabilize a laser. The high finesse cavity in use for stabilizing the TiSa of the $^{40}Ca^+$ experiment exhibits the following problems:

- The cavity is suspended with wires inside the vacuum chamber. One can clearly see the oscillation of this pendulum with its eigenfrequency in the error signal and the frequency of the laser. The decoupling of the cavity from the environment is not good enough.

- The short term temperature drift of the cavity of about 5 Hz/sec has to be improved.

The new high finesse cavity is made out of a ULE (ultra low expansion) spacer and high reflective mirrors optically contacted to it. ULE is a material which has a low thermal expansion coefficient specified to below $1 \cdot 10^{-8} \frac{1}{K}$ between 26 °C and 36 °C[1]. The cavity is vertically mounted at its center of mass to get a better suppression of vibrations (see chapter 3.2). It is a 77.5 mm long half symmetric resonator with one plane and one curved mirror with a radius of curvature $\rho = 500$ mm.

Additional efforts to further improve the setup will be presented in chapter 3.2. First a theoretical description of the cavity will be given.

3.1   Theoretical description of the cavity

The cavity consists of two mirrors at a distance L. Light with wavelength λ, that is sent onto one of the mirrors is partially reflected and partially transmitted.

The transmitted and the reflected fields are given by

$$E_t = t_1 \, E_i \quad and \quad E_r = r_1 \, E_i, \tag{3.1}$$

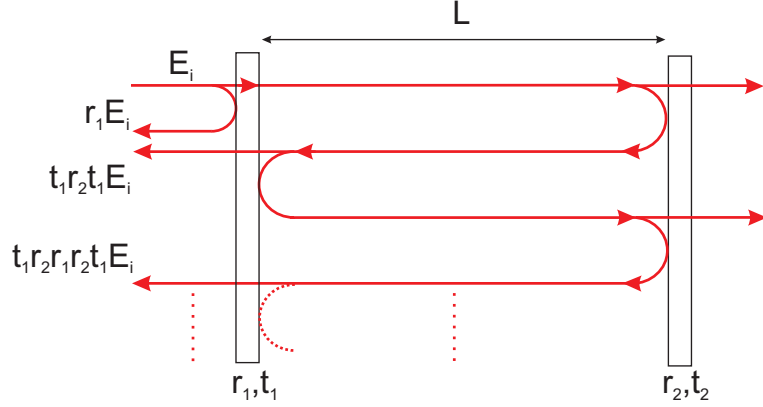
[1]specifications given by Corning

Figure 3.1: Multibeam interference of reflected and transmitted light in a cavity.

with $E_i = E_0 \, e^{i\omega t}$ being the incident light wave, r the reflection coefficient and t the transmission coefficient where

$$r^2 + t^2 = 1 \quad and \quad 0 \le r, t \le 1. \tag{3.2}$$

This equation is valid if the absorption in the mirrors is neglected. The transmitted light is split up again on the next mirror as illustrated in Figure 3.1. For calculating the reflection coefficient one has to take into account the phase Φ the light accumulates during the time T_ϕ while traveling from one mirror to the other and back again. Additionally one has to take into account the π phase shift of the light when it is reflected at the first mirror.

$$\Phi = \omega T_\phi = 2\pi \frac{2\,L}{\lambda} \tag{3.3}$$

So a factor of $e^{i\Phi}$ has to be added for every roundtrip of the light, and the total reflected field for a lossless cavity is then given by [24]

$$
\begin{aligned}
E_r &= E_i \left(-r_1 + t_1 r_2 t_1 e^{i\Phi} + t_1 r_2 r_1 r_2 t_1 e^{i2\Phi} + \ldots \right) &\tag{3.4}\\
&= E_i \left(-r_1 + \frac{t_1^2 r_2 e^{i\Phi}}{1 - r_1 r_2 e^{i\Phi}} \right). &\tag{3.5}
\end{aligned}
$$

In the special case of a symmetric cavity, $t_1 = t_2$, $r_1 = r_2$ this reduces to

$$E_r = E_i \, r \frac{e^{i\Phi} - 1}{1 - r^2 e^{i\Phi}}. \tag{3.6}$$

This term will be needed later, to derive the Pound Drever Hall locking signal (chapter 5.2). The reflected and transmitted intensities of a symmetric lossless cavity are

$$
\begin{aligned}
I_r &= I_0 \frac{4R \, \sin^2(\Phi/2)}{T^2 + 4R \, \sin^2(\Phi/2)} &\tag{3.7}\\
I_t &= I_0 \frac{T^2}{T^2 + 4R \, \sin^2(\Phi/2)} &\tag{3.8}
\end{aligned}
$$

with r^2=R the reflectivity and t^2=T transmission of a mirror.

Further important parameters for a cavity are the free spectral range (FSR) and the cavity linewidth. The FSR is the frequency distance between two TEM_{00} modes. The linewidth is the full width at half maximum (FWHM) of the transmission peaks. A laser is normally locked to a TEM_{00} mode of the cavity. Thus only stepwise changes of the laser frequency by one FSR are possible. With an AOM the laser frequency can be shifted relative to cavity mode. If the bandwidth of the AOM is as big as the FSR a continuous tuning from one mode to the next is possible. The FSR is given by the round trip time of the light

$$FSR = \frac{c}{2L}. \tag{3.9}$$

In the case of our cavity, L is specified to 77.5 mm so that the $FSR = 1.934\,GHz$ which has been verified by measurement (see chapter 3.4).

The finesse $\mathcal{F}$ is a measure for the average photon storage time in the cavity. It can be measured (see chapter 3.4) by determining the decay time τ of the light field leaking out of the cavity [20]. This is a so called ring down measurement.

$$\mathcal{F} = \tau \frac{c\pi}{L} = 2\pi\,\tau\,FSR \tag{3.10}$$

The finesse is directly related to the reflectivity of the mirrors [24]. This can be seen when calculating the linewidth from (3.7):

$$\mathcal{F} = \frac{\pi\sqrt{R}}{1 - R} = \frac{\pi\sqrt{1 - T}}{T} \tag{3.11}$$

If the losses A in the reflective surfaces are added, equation (3.2) changes to

$$R = 1 - A - T \tag{3.12}$$

Equation (3.11) also has to be modified which leads to

$$\mathcal{F} = \frac{\pi\sqrt{R}}{1 - R} = \frac{\pi\sqrt{1 - A - T}}{A + T} \tag{3.13}$$

The finesse of our cavity is specified between 300000 and 500000[2].

The linewidth of the cavity determines the slope of the locking signal and therefore the performance of the lock (see chapter 5.2). An accurate direct measurement of the linewidth $\Delta\nu$ of the cavity is hardly possible with an unstabilized laser but one can calculate it from (3.7) with the FSR and the finesse since

$$\Delta\nu = \frac{FSR}{\mathcal{F}} = \frac{1}{2\pi}\frac{1}{\tau}. \tag{3.14}$$

---

[2]Coating of the mirrors done by Advanced Thin Films

When building a cavity for laser stabilization the higher order modes should not lie close to the TEM_{00} mode. Especially the TEM_{10}, TEM_{11} and TEM_{10} can always be present to a small amount, even if the coupling to the cavity is good. Nearby other modes would distort the locking signal and therefore diminish the performance. Much higher order modes are not a problem, because one can make them vanish by a good cavity coupling. The frequency distance from one transverse mode to the other is given by [22]

$$\delta\nu = FSR\,(n+m+1)\frac{cos^{-1}(\sqrt{1-\frac{L}{\rho}})}{\pi}.$$ (3.15)

For our cavity parameters this leads to a $\delta\nu = 0.249$ MHz for adjacent modes. This means, that only high order modes around m + n = 8 might be a problem, but they can be easily suppressed by a good coupling. For coupling light into the cavity one has to sent the light exactly along the axes of the mirrors. The waist (w) of the beam has to be matched with the waist of the cavity mode. The radius ($1/e^2$ value of the intensity) of the cavity mode on the plain mirror side is given by [25]

$$w^2 = \frac{L\lambda}{\pi}\sqrt{\frac{r-L}{L}}.$$ (3.16)

For our cavity parameters this is

$$w = 205\,\mu m.$$ (3.17)

The waist of the incident beam can be adjusted to that value by choosing a suitable lems. The best thing to do is to collimate the beam and place a lens at the right distance. The equation to calculate the beam waist (W) for a given focal length f of the lens is given by [25]

$$W = f\frac{\lambda}{\pi\,w}.$$ (3.18)

This equation is valid for a collimated incident beam. With a f= 500 mm lens the incident beam has to have a radius of 566 μm. The beam waist W is given in the setup by the fiber and the fiber coupler (Figure 3.6). The focal length of the coupler that has to be used for collimating the beam can be determined with the help of the Schaefter & Kirchhoff manual [26] and is in this case a coupler with f= 6.2 mm.

3.1.1   Transient response of a Fabry-Perot cavity

The equations given for the cavity so far only hold for the case of a stationary light field. As already mentioned, if one switches off the light, it decays out of the cavity with a time constant τ related to the finesse of the cavity (see

equ. (3.10)). The light intensity transmitted through the cavity obeys equation (3.8) only if the frequency of the variation is below $1/\tau$. Houssin et. al. [27] calculated the frequency response of a cavity and found it to be a second order low pass in transmission, with a cut off frequency of

$$\nu_c = \frac{1}{2\pi} \frac{1}{\sqrt{\alpha}\,\tau} = \frac{1}{2\,\mathcal{F}} \frac{1}{\sqrt{\alpha}\,\tau} \qquad (3.19)$$

where $0 \leq \alpha \leq 1$ is the fraction of the transmitted intensity compared to the maximal intensity at resonance.

One can make the same calculation for the reflected light and it turns out, that the cavity behaves as a first order low pass with a cut off frequency

$$\nu_c = \frac{1}{2\pi\,\tau} = \frac{1}{2\,\mathcal{F}\,\tau} \qquad (3.20)$$

which is equal to half the cavity linewidth. At low frequencies the transfer function for the reflected light is proportional to the finesse. Above the cut off frequency, the cavity integrates over the frequency fluctuations and thus behaves as a phase discriminator. At first, it looks like as if the bandwidth of the detectable frequency variation of the light was limited by the $1/\mathcal{F}$ relation of Equation 3.20. Especially high finesse cavities which are necessary for ultra stable lasers (see chapter 5.2) have low cut off frequencies. But the unity gain frequency of the cavity stays the same because the low frequency gain increases as much as the cut off frequency goes down. The transition from the frequency to the phase sensitive regime is smooth. A locking technique using the reflection will not be limited by this low pass behavior if the servo electronics can deal with the 90° phase-change [7].

3.2 Mechanical setup

For constructing a narrowband laser, a reference cavity with high mechanical stability is absolutely necessary. Several approaches have been made to prevent changes of the cavity length caused by acoustic and seismic noise. They have been based on active vibration isolation or mounting the cavity on a system with very low eigenfrequency. The design [28] used here exploits the fact, that if the cavity is accelerated along the cavity axes and the support points are arranged in the symmetry plane between the two mirrors, each half of the cavity is deformed in such a way that the distance between the mirrors does not change. The decrease of length on one side is compensated with an increase on the other. The mounting configuration and a schematic picture of the whole setup can be seen in Figure 3.2.

3.2.1 Vibration isolation

The whole setup was built on an optical table which rests on a 32 t concrete block floating on air pistons. This table has a very low eigenfrequency, which already suppresses seismic noise. Additionally sorbothane has been put between
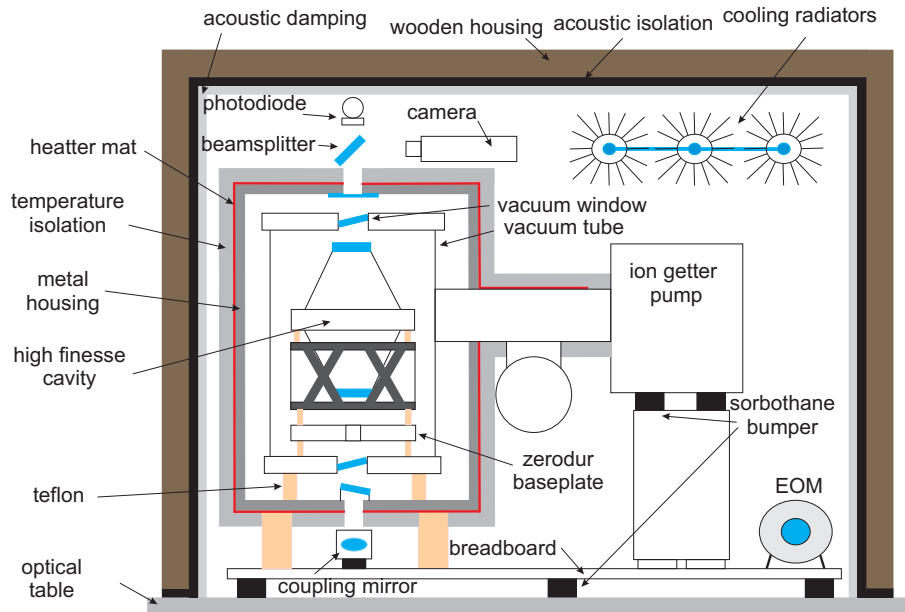
Figure 3.2: Mechanical layout of the cavity setup. The cavity is mounted on teflon sticks resting on a zerodur baseplate. The cavity is surrounded by a vacuum chamber and a metal housing. The metal housing is temperature stabilized. A photodiode and a camera monitor the transmission of the light through the cavity. The radiators are used to additionally temperature stabilize the wooden box around the whole setup. This box serves for acoustic shielding and temperature isolation. The whole setup is mounted on a breadboard

the breadboard and the lab table. Sorbothane is a polymer which is capable of absorbing shock and vibrations from around 200 Hz up to 10 kHz. If the design is made carefully so that the compression of the pads has the right amount, a vibration damping of up to 20 dB is possible (shown in Figure 3.3). The measurement was performed with a piezoresistive accelerometer and the FFT analyzer. The accelerometer can be used to measure frequencies up to 6 kHz because it has some intrinsic resonances at around 8 kHz and a strong low pass characteristics above 10 kHz which would spoil the measurement. The vibrations that can be seen are due to background noise in the lab which couple into the surface of the optical table. The high peak in the sorbothane graph at 50 Hz is a ground loop problem and is not a real resonance.

Acoustics can directly couple into the setup via air. For this reason a wooden box with an additional layer of sound blocking material, has been built around the vacuum system. The rubber like material[3] alone guarantees a suppression of 25 dB in the kHz regime and combined with the heavy wooden box around 30 dB can be achieved. Additionally a sound absorbing material has been put on the wall of the box to suppress the formation of standing waves. The acoustic
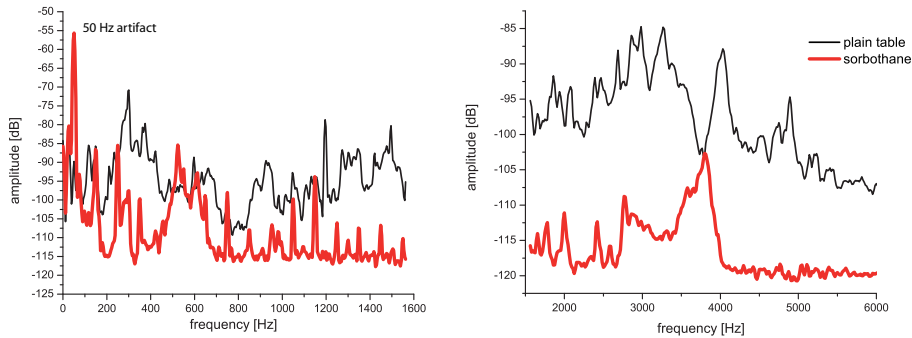
---

[3]Auralex Sheetblok

Figure 3.3: Vibrations on the lab table. With the help of sorbothane the vibrations coupling into the breadboard can be reduced by 20 dB. Sorbothane only works for frequencies between 200 Hz and 10 kHz

noise inside and outside the wooden box was measured with a microphone[4] and the FFT analyzer. The microphone has a linear response from 10 Hz to 10 kHz. The result of the measurement can be seen in Figure 3.4.
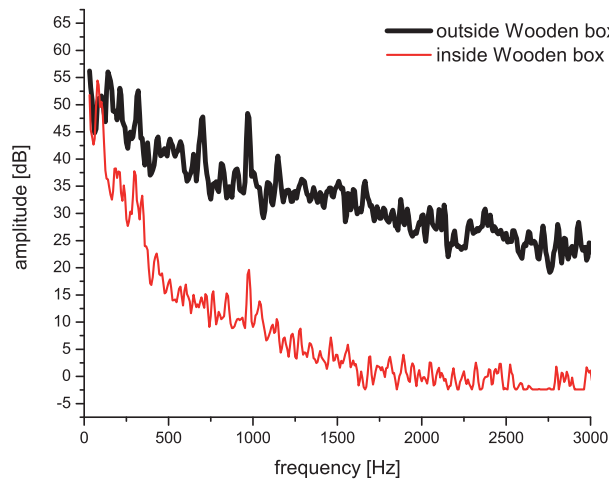

Figure 3.4: Acoustic noise spectrum inside and outside the wooden box. Noise is suppressed inside the wooden box by 30 dB above a frequency of 500 Hz.

The acoustic noise is suppressed by 30 dB above a frequency of 500 Hz. The noise below 500 Hz is produced by the Verdi power supply and the air condition in the basement. Acoustic shielding of these sources might help to reduce the noise further.

3.2.2   Temperature stabilization

The spacer of the cavity is made out of ULE and therefore has a low thermal expansion coefficient. However a temperature change of 1 K would still change

---

[4]ICP microphone MPA201

the frequency of the cavity by 4 MHz. The lab temperature is only stable within 1 K, so an additional stabilization is required to achieve the desired low drift rates. The cavity is placed inside a vacuum chamber, held at a pressure of about 10^{-8} mbar where it rests on teflon sticks and a zerodur baseplate. Due to the vacuum heat convection inside the cavity is suppressed. The teflon suppresses heat conduction between the cavity and the vacuum chamber through the mounting. The zerodur baseplate, a material with a thermal expansion coefficient below $10^{-6}\frac{1}{K}$, is there to build a buffer between the ULE and the metal. This means that if the position of the mounting holes in the metal changes due to temperature the shear created by that is imposed on the zerodur baseplate. The cavity itself experiences a much lower mechanical stress. So deformations of the vacuum tank don't contribute to the frequency changes.

Pressure variations would change the refractive index and thus the effective length of the cavity. The vacuum chamber around the cavity also solves this problem.

The vacuum tank is surrounded by a metal housing with heater mats attached to the housing. The heater mats are used to temperature stabilize the metal housing and therefore the vacuum tank. The housing is stabilized to $\approx$ 30 °C so that less heating results in an effective cooling. Six NTC (negative temperature coefficient) resistors, one in each wall of the metal housing are used to measure a mean value of the temperature. This signal is used for the feedback. An additional PT 100 for a direct temperature measurement was glued to the vacuum chamber. A further 12 mm layer of polystyrene was added on top of the heater mats for additional isolation. To prevent chimney effects the holes for the light transmission were closed by glass plates. These plates were mounted under an angle to the incident beam so that no etalon effects caused by parallel surfaces can occur. Also the wooden box for the acoustic isolation provides some thermal isolation.

With this setup a suppression of temperature fluctuations by a factor of 50 to 100 is possible. To achieve a bigger suppression cooling radiators were placed inside the wooden box which are water cooled via peltiers. A measurement of the temperature inside the wooden box and the cavity vacuum chamber, both with a PT 100, can be seen in Figure 3.5.

Both of the measurements shown in Figure 3.5 are quite noisy, which is due to RF sources (trap drive, EOMs & AOMs) near the sensors. The fluctuations of the PT 100 on the vacuum chamber are smaller compared to the PT 100 lying in the wooden box because it is shielded by the metal housing from the RF sources. By averaging one can get rid of these fast fluctuations and is then able to see, that the temperature on the vacuum tank stays within 4 mK over the course of three days. The inside of the wooden box is stable to 100 mK while the temperature of the lab changes by 700 mK in a 24 h cycle. One can still see some of these 24 h fluctuations in the signals.

These fluctuations are caused by the servo circuit itself. It was observed that temperature changes of the servo circuit result in changes of the cavity temperature. A 1 K change of the servo changed the cavity temperature by 10
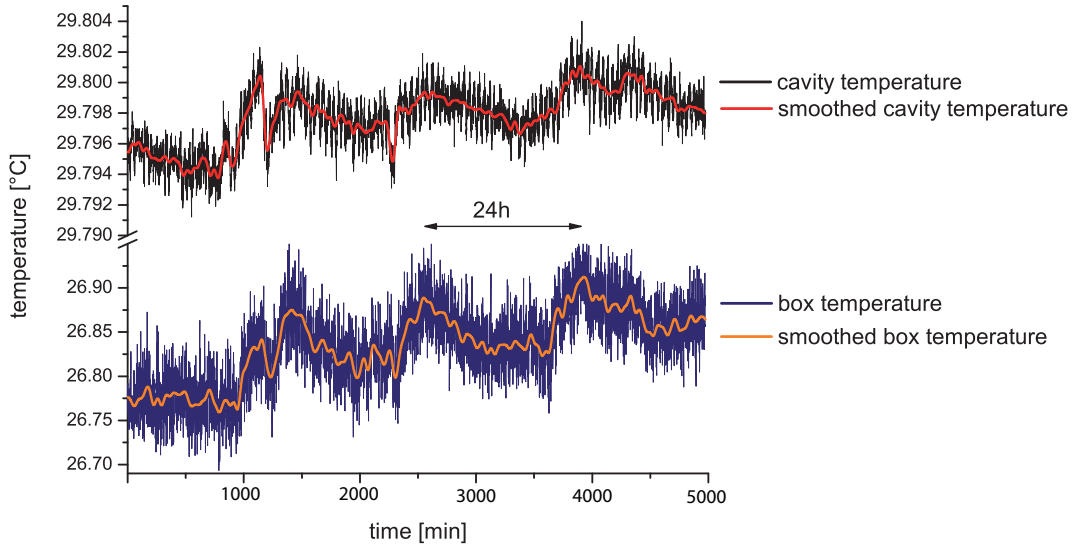
Figure 3.5: Measurement of the temperature of the wooden box and the vacuum chamber. Temperature variations on the vacuum chamber are around 4 mK. Variations in the wooden box are 100 mK. The temperature of the lab changes by approximately 700 mK on a 24 h cycle.

mK. To get rid of this effect, it is planned to stabilize the temperature of the servo itself so that it causes no changes.

Measurements of the drift of the cavity frequency due to temperature changes are discussed in chapter 3.5 but this measurement was done without the cooling radiators and the temperature stabilization of the servo. It will have to be repeated for the improved system.

3.3 Optical setup

Light is sent via a fiber from the TiSa to the high finesse cavity. Additional optical elements are needed for locking the laser to the cavity (Figure 3.6).

The output coupler of the fiber is tuned in such a way, that a collimated beam exits, which is important for the cavity coupling. Then the beam passes a polarizer[5] with an extinction ratio of 10^{-6}. It is needed to get a well polarized beam parallel to the optical axes of the subsequent EOM[6] to suppress unwanted effects (chapter 5.2.3).

A radio frequency of 17.78 MHz is applied to the EOM to imprint sidebands on the light, which then create the error signal (see chapter 5.2). The necessary voltage is generated by a resonant circuit. The coil has to be mounted close to the EOM in order to get a good quality factor and to minimize stray RF fields.

---

[5] Glan Thompson, manufactured by B.Halle Nachfl. GmbH
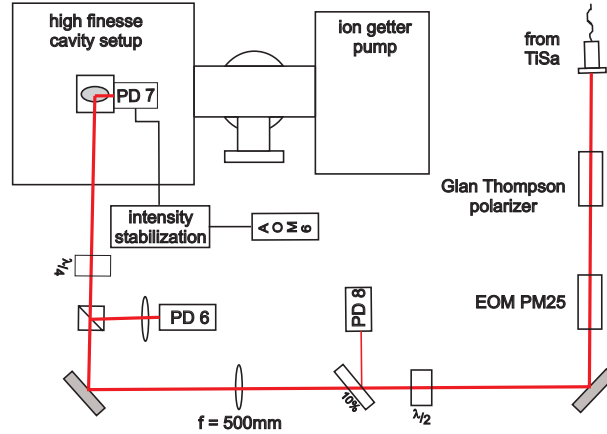[6] Linos, model PM25

Figure 3.6: Optical setup around the high finesse cavity. The light is sent through a fiber and enters a polarizer followed by an EOM. The EOM is used for creating sidebands on the light. The light then passes a polarizing beam splitter and a $\lambda/4$ plate. The back reflection is detected by PD 6. PD 8 is used to optimize the fiber coupling. PD 7 detects the light transmitted through the cavity.

The light is then sent through a polarizing beam splitter and a $\lambda/4$ plate to the cavity. The back reflection is detected by PD 6[7]. This signal is used for locking the laser to the cavity.

The temperature of the mirror substrates changes if light is sent through the cavity. This is due to the absorption of the substrate material. A changing light intensity would thus result in a changing cavity length. To stabilize the intensity the transmitted light through the cavity is detected by PD 7[8]. The intensity is regulated in front of the fiber guiding the light to the breadboard (see Figure 4.1 and chapter 4).

PD 8 is used to optimize the fiber coupling.

3.4   Measuring the cavity parameters

3.4.1   Free spectral range

To characterize the cavity the FSR has been measured. This parameter is needed to determine the finesse of the cavity and to know how much the frequency of the laser changes if it is locked to a different mode. Two different cavity modes have too be used to bridge the frequency gap between $^{40}Ca^+$ and $^{43}Ca^+$. So the FSR has to be known to a few MHz accuracy to set the laser to the right transition frequencies.

The measurement was done by locking the TiSa to three different modes of the cavity and measuring the beat signal with the $^{40}Ca^+$ TiSa. The beat

---

[7]Similar to New Focus, model 1801-FS Si 125-MHz
[8]PD 7, 8 . . . Thorlabs, model SM05PD1A

was detected with a fast photodiode[9] and a spectrum analyzer locked to the 10MHz reference. First the beat frequency was measured for a laser wavelength of 729,147 nm. Then the laser was detuned one mode to the blue and then one mode to the red. The resulting beat frequencies can be seen in Figure 3.7
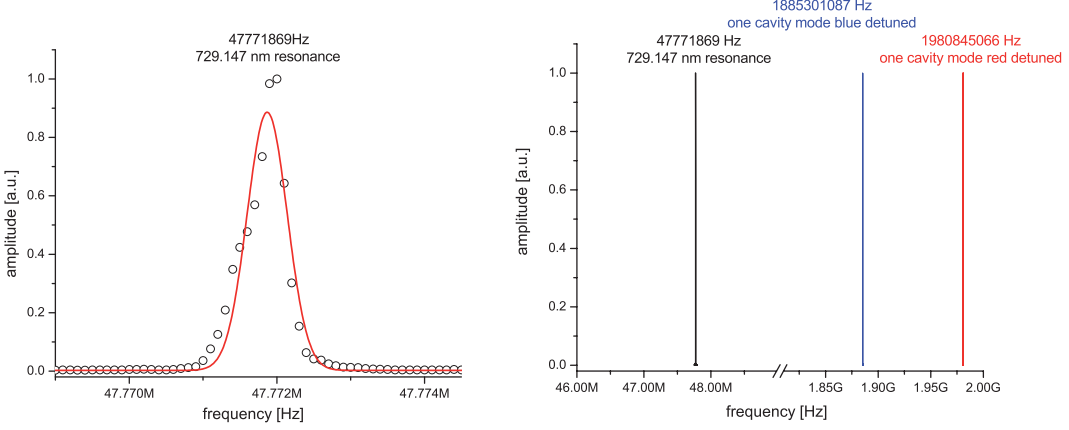
Figure 3.7: Left plot: cavity resonance for a laser frequency of 729.147 nm. Right plot: beat frequencies for the three cavity modes: 729.147 nm cavity resonance, one mode blue detuned, one mode red detuned

To each of the lines a Gaussian fit has been made, to determine the center-frequency of the peak. Every series was done three times so the FSR could be determined six times. The resulting value is

$$FSR = 1.93307307\,GHz \pm 470\,Hz \tag{3.21}$$

at a wavelength of 729.147 nm. This is slightly off if compared to the expected FSR calculated with the cavity length of l = 77.5 cm. The length of the cavity calculated with the measured FSR is

$$l = 77.542971\,mm \pm 19\,nm \tag{3.22}$$

which means, it differs by 43 μm from the specified length of the cavity spacer. This difference might be explained by adding the additional length Δl, created by the curvature of the mirror, to the total length of the cavity. The diameter of the mirror is 1/2 inch and with the given radius of 500 mm this leads to

$$\Delta l = 40\,\mu m \tag{3.23}$$

which reduces the discrepancy.

---

[9]16 GHz Hamamatsu photodiode G4176, Miteq Bias-Tee 40 GHz BT 4000, Miteq amplifier AFS42-00101200

3.4.2   Finesse and linewidth

The finesse is usually measured by scanning a laser over the cavity resonances and detecting the transmitted signal. By determining the linewidth of the resonances and the free spectral range from this signal one can then calculate the finesse. This method is only applicable if the linewidth of the laser is at least 10 times smaller than the linewidth of the cavity. This is quite difficult in our case, because one would need a laser with a few 100 Hz width. As an alternative the finesse can be determined by measuring the decay time of the light stored in the cavity. This is done by tuning the laser to a resonance which means the cavity is filled with light and a part of it is transmitted. When the transmitted light reaches a certain level the laser is switched off fast and an exponential decay in the intensity of the transmitted light can be seen. The switching has to be done much faster than the decay time, otherwise the decay is governed by the switching time.
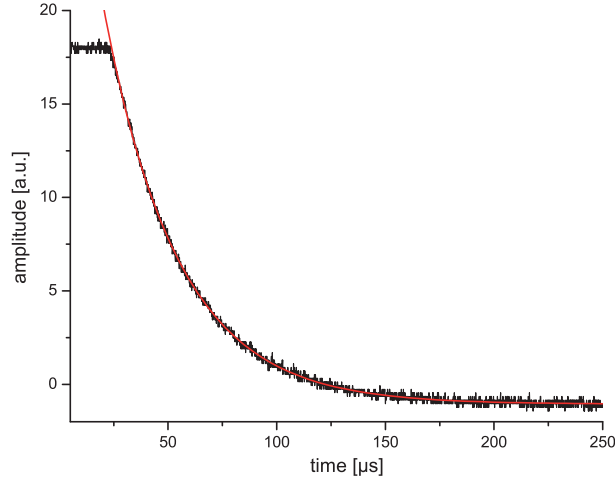

Figure 3.8: Intensity of the light field decaying out of the high finesse cavity. A decay time of 33.88 μs was measured

Five sets of data were taken with the help of a storage oscilloscope and a fit was made to them to determine the decay time to

$$\tau = 33.88 \, \mu s \pm 0.07 \, \mu s \tag{3.24}$$

which leads to a finesse calculated with the measured FSR of

$$\mathcal{F} = 411540 \pm 350. \tag{3.25}$$

This measurement has to be done with a laser stabilized to a linewidth in the order of the cavity linewidth. This can be easily achieved by locking the laser to an external medium finesse cavity. If the laser is broader, additional effects influencing the signal have to be taken into account. These effects were observed when the TiSa was used in its standard configuration with a linewidth of 500 kHz to do the measurement. This can be seen in Figure 3.9
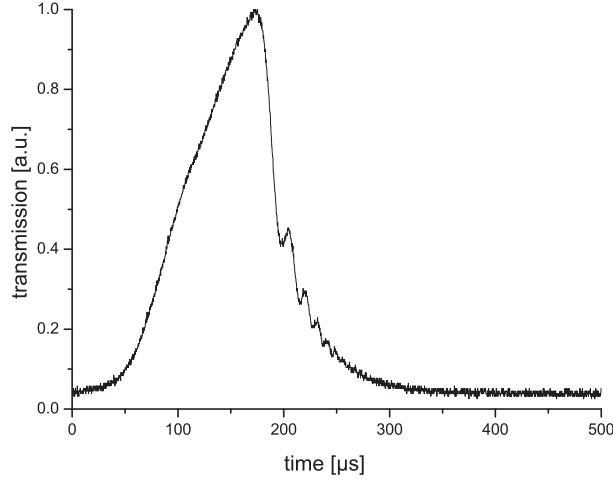
Figure 3.9: Transmission signal with interference effects due to an unstable laser. Light stored in the cavity interferes with light of different frequency sent to the cavity.

The behavior shown in Figure 3.9 can be explained by interference effects. When the laser comes into resonance with the cavity, light is stored in the cavity. If the laser then changes its frequency faster than the decay time stored light leaking out of the cavity interferes with light directly reflected from the input mirror. Destructive and constructive interference cause oscillations in the transmitted signal. Another interesting phenomenon occurs when the incident light is switched in phase by π. Due to destructive interference the decay time is twice as fast. This behavior has already been investigated [29] and theoretically explained [30].

With the known decay time, or by relating the FSR and the finesse one can calculate the linewidth of the cavity to

$$\Delta\nu = 4.698\,kHz \pm 4\,Hz. \tag{3.26}$$

3.5   Measured drift rates of the high finesse cavity

For the experiment it is important that the frequency of the 729 nm laser is constant during the experiments so that a coherent manipulation of the atoms is possible. For that reason the frequency drift of the cavity the laser is locked to has to be as low as possible. The drift was determined by measuring the resonance frequency of the $S_{1/2}$, m=-1/2 to $D_{5/2}$, m=-3/2 transition in $^{40}Ca^+$. The frequency of the AOM tuning the laser into resonance with the cavity is plotted in Figure 3.10. This measurement has been repeated whenever an ion was in the trap for a period of one month.

The frequencies plotted in Figure 3.10 are AOM frequencies. The AOM is used in a double pass configuration. Thus, to get the real drift, one has to double the frequencies. The resulting drifts are on average
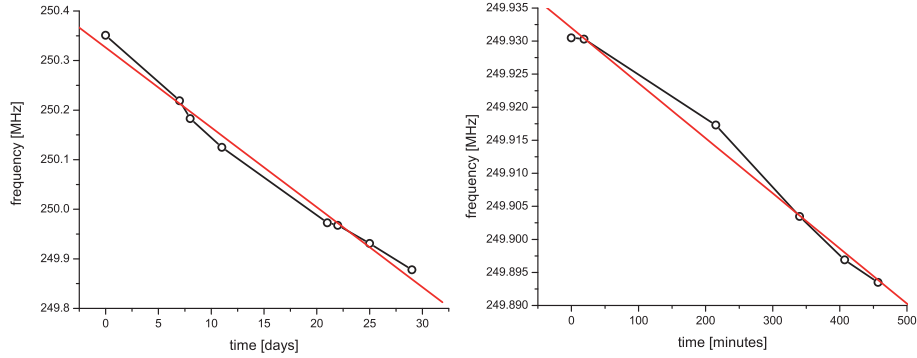
Figure 3.10: Left plot: drift of the cavity over one month period starting with the 30.05.06. The average drift was 0.37 Hz/s. Right plot: Average cavity drift of 2.77 Hz/s on the 26.06.2006.

$$0.37 \text{ Hz/s}$$

over a period of one month and

$$2.77 \text{ Hz/s}$$

on the 26.06.06 over a period of 7 hours. One can see that there is a constant low drift over time which can be compensated quite easily by applying a constant drift to an AOM. The higher value of the 26th of july was one of the biggest rates measured up to now and is most probably caused by the insufficient temperature stabilization at that time. Meanwhile the temperature stabilization has been improved but up to now no new drift measurements have been done. It should be mentioned, that the transition measured is sensitive to magnetic field fluctuations and since there is no system canceling those, magnetic field drifts might also contribute to the change in resonance frequency. The drift measurement will be repeated on a magnetic field insensitive transition of $^{43}Ca^+$ to get values which are not influenced by these effects.

Furthermore it has been found, that the frequency of the cavity changes with temperature roughly by 17 MHz/K. This corresponds to an expansion coefficient of $8 \cdot 10^{-8}$ which is above specifications. The group of Theodor Hänsch, who is using the same type of cavity also reports a higher expansion coefficient as specified [31].

Chapter 4

Optical setup for the 729 nm light

The optical setup has been designed to be compatible with the requirements listed in chapter 1.4. The light is manipulated with AOMs and sent through fibers to the cavity, the experiment, a wavemeter and to the $^{40}Ca^+$ experiment.

4.1 Description of the parts

Figure 4.1 displays the optical setup needed for the operation of the TiSa in the experiment. It consists of three main parts. $\lambda/2$ plates and polarizing beam cubes are used to distribute the light:

- In the "experiment branch" the light to manipulate the ions is generated. AOM 1 stabilizes the intensity of the light coming out of the laser. The double pass configuration around AOM 2[1] is able to switch the frequency of the laser light within a few μs. AOM 3 and 4 are used for switching.[2] By tuning AOM 2 the frequency of the light can be changed by more than the required 100 MHz. The light is sent to the experiment through two fibers. One light beam enters the trap horizontally and the other under an angle of 45° from below. A small part of the laser light is sent by a fiber to the wavemeter to determine the wavelength.

- In the "lock branch" the laser frequency is shifted to bring it into resonance with a cavity mode. The double pass configuration with AOM 5[3] allows us to change the detuning of the laser by 2 GHz. With this AOM a continuous tuning from one TEM_{00} cavity resonance to the other is possible. The PD 4[4] checks whether the power sent towards AOM 5 is not too high, because the AOM can stand only 30 mW for the chosen

---

[1] Brimrose, 270 MHz, model TEF-270-100-800
[2] AOM 1, 3, 4, 6, 7 . . . Crystal technology, 80 MHz, model 3080-120
[3] Brimrose, 1.5 GHz, model GPF-1500-100
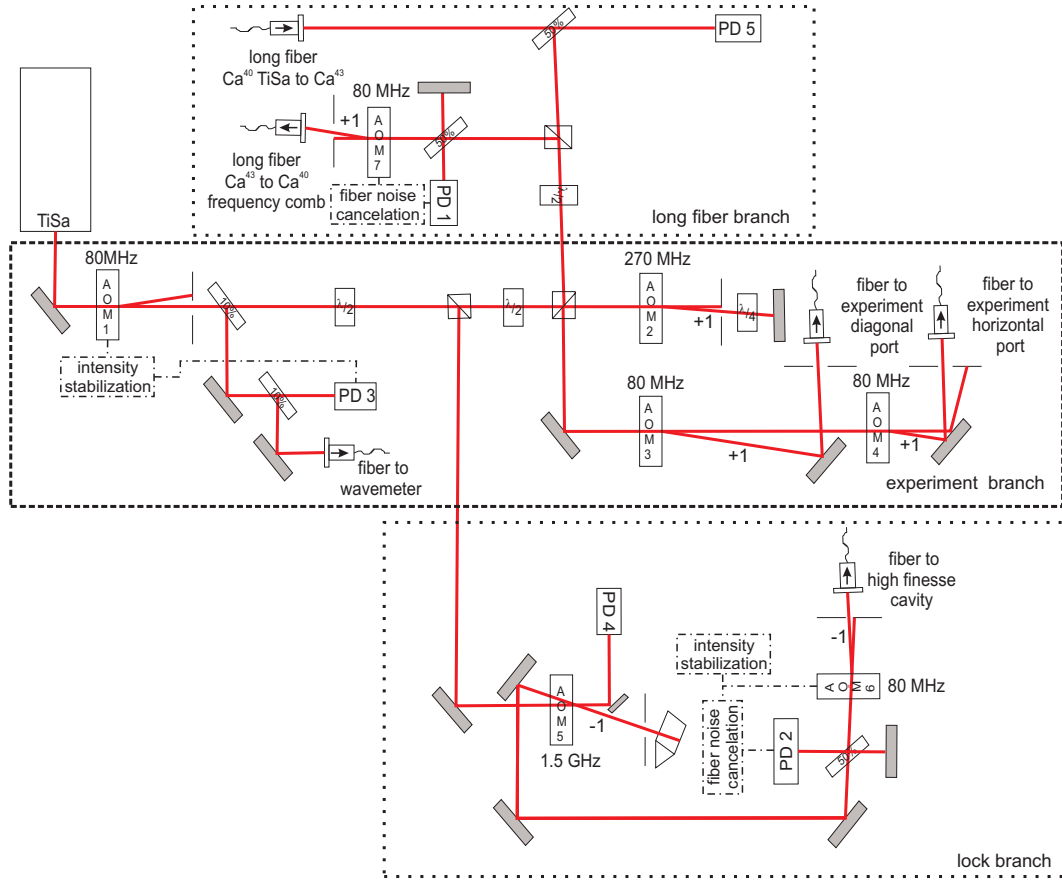[4] Thorlabs, model SM05PD1A

Figure 4.1: Optical setup for the generation of the 729 nm light. It is divided in three different branches: The "experiment branch" to generate the light for the experiment. The "lock branch" to pick off light for a lock to the cavity. The "long fiber" branch to sent light to the $^{40}Ca^+$ frequency comb and to do the beat measurement between the ultra stable TiSa lasers.

beam diameter. AOM 6 serves for stabilizing the light intensity transmitted through the cavity (see chapter 3.3. The efficiency of AOM 5 is not constant over its bandwidth and changes with temperature which is also compensated with AOM 6.

In addition, AOM 6 together with PD 2[5] is responsible for the fiber noise cancellation (chapter 4.3) of the fiber guiding the light to the cavity.

- In the "long fiber branch" the light is sent over a 500 m long fiber[6] to the frequency comb, after passing a fiber noise cancellation consisting of AOM 7 and PD 1. A part of the light together with light coming from the $^{40}Ca^+$ TiSa is sent onto a fast photodiode[7] to measure the beat of

---

[5]PD 1, 2 . . . similar to New Focus, model 1601-FS-AC Si 1-GHz

[6]Laser 2000: 2 x standard single mode, 2 x single mode 780-970 nm, 1 x single mode 600-760 nm, 1 x PM - fiber 800-980 nm, 1 x PM - fiber 630 - 780 nm

[7]16 GHz Hamamatsu photodiode G4176, Miteq Bias-Tee 40 GHz BT 4000, Miteq amplifier

the two lasers. This setup is used to determine the FSR of the cavity and the linewidth of the lasers (seen chapter 3.4.1 and chapter 6.2).

The light entering the different fibers has the following frequencies:

$$
\begin{aligned}
\nu_{exp} &= \nu_{laser} + 2\,\nu_{AOM2} + 80\,\text{MHz} \\
&= \nu_{lock} + 2\,\nu_{AOM2} + 2\,\nu_{AOM5} + 160\,\text{MHz} \\
\nu_{lock} &= \nu_{laser} - 2\,\nu_{AOM5} - 80\,\text{MHz} \\
\nu_{long} &= \nu_{laser} + 80\,\text{MHz} \\
&= \nu_{lock} + 2\,\nu_{AOM5} + 160\,\text{MHz}
\end{aligned}
$$

ν_{lock} has to match the resonance frequency of the cavity, so that the laser can be locked to it (see chapter 5.2).

4.2 Intensity stabilization

The output power of the TiSa can vary over time because of temperature changes, acoustic vibrations and settling of mirrors. There is also the 2 kHz amplitude modulation produced by the etalon lock. The light intensity has to be kept constant for the following reasons:

- If the laser is used to coherently excite an atomic transition, the Rabi frequency is linearly dependent on the electric field strength of the light [20].

- For stable locking of the TiSa the light power sent to the cavity has to be kept constant because the slope of the error signal depends on the light power.

The setup for an intensity stabilization is shown in Figure 4.1. The intensity variations are detected by PD 3[8]. This signal is fed back to AOM 1 by a PI controller[9]. This PI controller changes the RF output power of the AOM driver. If the photodiode detects more than the desired light power the RF power is increased and more light is taken out of the zeroth order beam into the first order. For a light intensity below the setpoint the RF power is decreased transferring light from the first into the zeroth order. This stabilizes the zero order light intensity. To get a good stabilization the setpoint for the servo is chosen to be around 90 % of the output power so that it can compensate power drops of up to 10 % and power increases. The amplitude noise spectrum of the TiSa with and without stabilization can be seen in Figure 4.2.

The servo loop bandwidth of about 100 kHz is sufficient to suppress power fluctuations which create the biggest disturbances at frequencies below 10 kHz. Fluctuations in the kHz regime are reduced by a factor of ten whereas changes over minutes and hours can be reduced to zero.

AFS42-00101200

[8]Thorlabs, model SM05PD1A
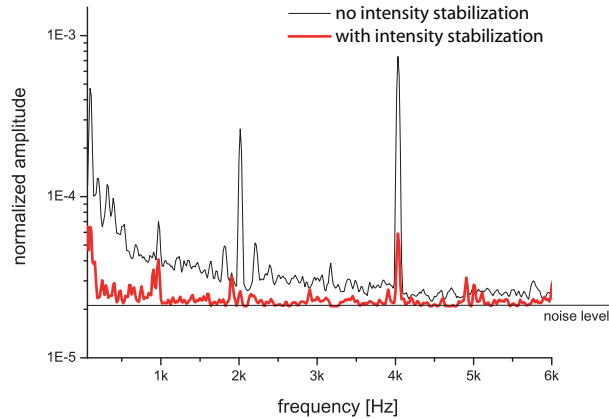[9]SRS SIM960 Analog PID Controller

Figure 4.2: TiSa amplitude noise spectrum with and without intensity stabilization. Peaks at 2 kHz and 4 kHz dominate the spectrum. They are produced by the electronics of the thick etalon lock. The intensity stabilization reduces them by an order of magnitude.

4.3   Fiber noise cancellation

If a laser beam passes through an optical fiber its spectrum broadens. This is caused by changes in the index of refraction due to sound waves, changes in the pressure and temperature. This effect broadens the spectrum by about a kHz which causes the following problems:

- A beat measurement of two narroband lasers, where one or both beams pass fibers, will be dominated by the broadening of the fiber. Thus the frequency stability of the laser cannot be reliably measured.

- Light has to be sent to a cavity to stabilize the laser to it. If this is done by a fiber the frequency noise of the fiber will be transferred to the laser frequency.

The setup shown in Figure 4.1 gets rid of this effect by interferometrically stabilizing the optical length of the fiber. It consists of AOM6, PD2 and the 50:50 unpolarizing beam splitter. This setup uses the approach presented in a paper [32] published by the group of John Hall.

4.3.1   Mode of operation

The light is sent through the AOM before it enters the fiber. Part of the light (4% because of 0° angle of the fiber end) is backreflected from the other end and passes again the AOM. In that way one has a double pass setup where the beat note between the light passing the AOM twice and the unmodulated light can be detected. In our setup the beat is measured at a frequency of 160 MHz because an 80 MHz AOM is used.

The beat-signal is then mixed down to DC with a stable reference[10] running

---

[10]Rohde & Schwarz SML01 signal generator, locked to a 10 MHz reference

also at 160 MHz. The phase difference between the reference and the beat signal is then fed back to the VCO which drives the AOM. The servo tries to set the phase difference, $\phi_{\text{AOM}} - \phi_{\text{fiber}}$, to zero and thus compensates the phase fluctuations caused by the fiber. A block diagram of the setup can be seen in Figure 4.3.
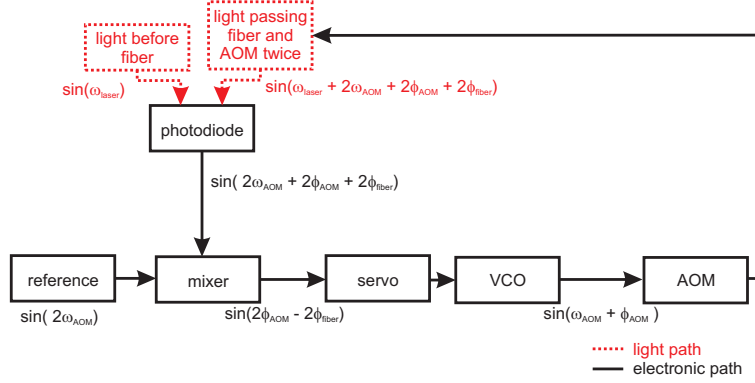

Figure 4.3: Scheme of the fiber noise cancellation. The servo tries to set the phase difference between reference and beat signal to zero. In that way the noise caused by the fiber is canceled.

A circuit diagram of the fiber-noise-cancellation can be found in appendix B. The cancellation only works, if the fiber length is shorter than the coherence length of the laser. If this is not the case, the servo does not receive a signal on which it can lock to. This effect was observed when stabilizing the 500 m long fiber. When the TiSa laser was only stabilized with the Coherent lock the fiber noise cancellation did not work. The linewidth of the laser is in this case only $\Delta\nu \approx 500$ kHz which means the coherence length

$$l = \frac{c}{2\pi\Delta\nu} \tag{4.1}$$

is roughly 100 m. This is much shorter than the fiber length. When the laser was stabilized to the high finesse cavity, the coherence length was larger than 450 km which made it then possible to run the fiber noise cancellation.

4.3.2 Effect of the fiber noise cancellation

Spectra of the beat frequency were recorded to show the effect of the fiber noise cancellation. Two different spectra are shown in the left and right part of Figure 4.4. The black curve was measured without a servo. The AOM was driven by a stable reference[11]. Thus the broadening of the spectrum is dominated by the fiber and not by a drift of the oscillator driving the AOM. The red curve was measured with the fiber noise cancellation switched on. All spectra were recorded with a spectrum analyzer in FFT mode.

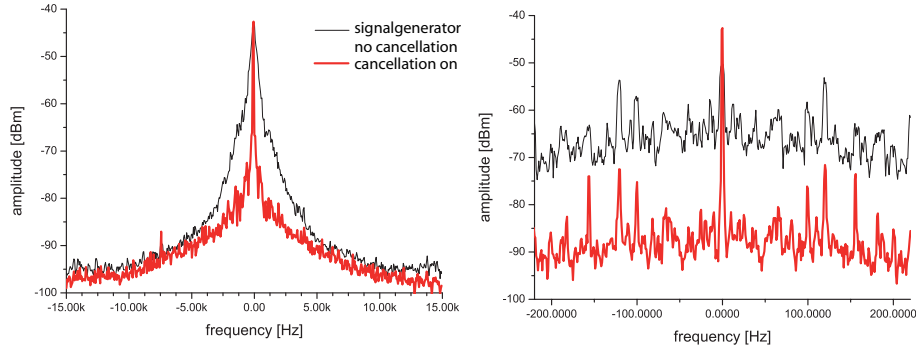[11]Rohde & Schwarz SML01 signal generator, locked to a 10 MHz reference

Figure 4.4: Spectra of the fiber noise for the cavity fiber with and without cancellation. The fiber noise cancellation is able to reduce the noise by 25 dBm between 0 and 2 kHz. Left plot: frequency span of 30 kHz around the beat frequency. Right plot: frequency span of 400 Hz around the beat frequency with minimal resolution bandwidth of 1 Hz

Figure 4.4 demonstrates that the fiber noise cancellation reduces the phase noise of the spectrum by 25 dB between 0 and 2 kHz. The reduction goes down to a few dBm above 5 kHz. The resonance peaks visible in the right part of Figure 4.4 are due to acoustic noise in the lab. The width of the recorded beat is limited by the resolution of the spectrum analyzer.

For a better resolution the signal was mixed down to around 1 kHz for measuring it with the FFT analyzer. The beat recorded in such a way for the 500 m long fiber link can be seen in Figure 4.5. The amplitude was normalized to one and a Gauss fit was made to the data, with a resulting linewidth of the peak of 0.27 Hz. This width was not limited by the resolution of the FFT analyzer which was 62 mHz. These measurements show, that the fiber noise cancellation is able to suppress the broadening of the laser spectrum by at least 25 dBm in a frequency range of 2 kHz around the carrier. The stabilized fiber adds 0.27 Hz to the linewidth of the light entering the fiber. The cancellation works for distances up to 500 m if the coherence length of the light is long enough.
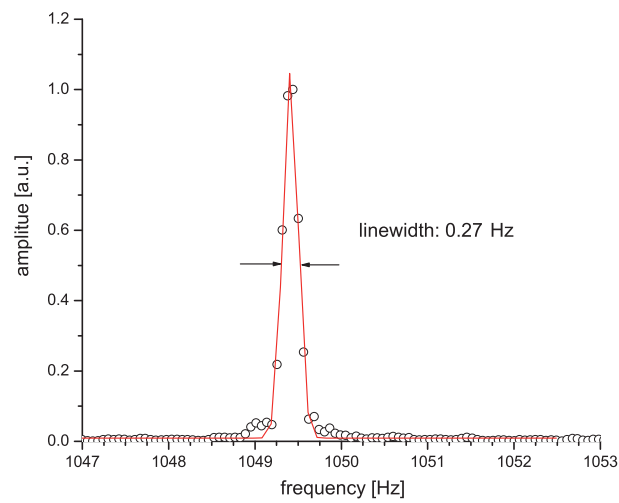
Figure 4.5: Mixed down fiber noise cancellation spectrum for the 500 m fiber. The width of the peak of 0.27 Hz was not limited by the resolution bandwidth of the FFT analyzer (62 mHz).

Chapter 5

Frequency stabilization of the TiSa laser

The first section introduces the basic principle of feedback and PI controllers. Then the principle of the Pound-Drever-Hall (PDH) technique for stabilizing lasers will be explained. The last section deals with the actual setup of the feedback and gives an insight to the required electronics.

5.1   Introduction to feedback

In nearly all branches of experimental physics some kind of stabilization is required because most of the time physicists deal with unstable systems. Temperature stabilization, the control of the magnetic field of a coil and the stabilization of lasers are just a few examples to be mentioned. Here the basic ideas as well as some rules for the design of a servo are introduced. A more advanced and thorough overview is given in several books [33],[34] and articles [35].

5.1.1   Servo basics

The goal of a feedback loop is to have the output signal $Y_{out}(s)$ of a system faithfully follows the input signal $Y_{in}(s)$ and any disturbances $Z(s)$ influencing the system get canceled. The system is described by its complex transfer function $S(s)$ and the servo is represented by $G(s)$. The functions $Y_{in}(s)$, $Y_{out}(s)$ and $Z(s)$ are the Laplace transform of the real signals $y_{in}(t)$, $y_{out}(t)$ and $z(t)$ [35], [34]. For this discussion it is sufficient to set $s = i\,\omega$, where ω is the angular frequency. Figure 5.1 shows the schematic block diagram of a general servo system.

The transfer function of this circuit, which determines the capability of the system to follow the input signal, is described by

$$H(s) = \frac{Y_{out}(s)}{Y_{in}(s)} = \frac{G(s)\,S(s)}{1 + G(s)\,S(s)}. \tag{5.1}$$
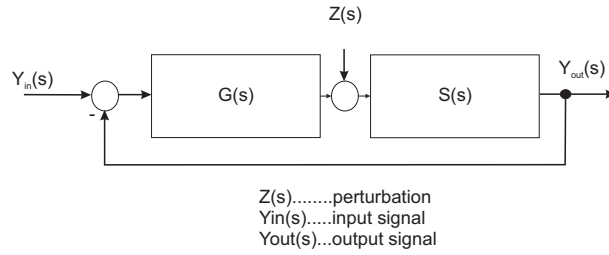
Figure 5.1: Basic servo loop with Servo G(s) and system S(s).

Note the negative sign at the feedback node which implies that $Y_{out}(s)$-$Y_{in}(s)$ is fed back into the servo. If the output signal is below the setpoint, given by the input signal, the output signal is pushed towards the desired value. This implies that the output signal is able to follow changes of the input faster as compared to the system without feedback. This is illustrated in Figure 5.2 where the system with feedback reacts faster.

Another important parameter is the effectiveness of the servo for canceling perturbations. The transfer function that characterizes this is given by

$$H'(s) = \frac{Y_{out}(s)}{Z(s)} = \frac{S(s)}{1 + G(s)\,S(s)}.$$ (5.2)

For laser stabilization this is the interesting term because disturbances have to be canceled fast and complete. We are not interested in optimizing the properties of H(s) as the setpoint is usually kept constant. In equation 5.2 one can already see, the bigger G(s) is, the better perturbations are canceled.

The effects of a servo will be demonstrated with a small and very simple example. For the system a lowpass of first order with a cut off frequency ω_0 is used. It has a transfer function of

$$S(s) = \frac{1}{1 + \frac{s}{\omega_0}}.$$ (5.3)

Two types of servos will be used to show the different behavior off the pure system and the system in a servo loop. One servo will be pure proportional (P-servo) with

$$G(s) = k_p$$ (5.4)

and the other will be a proportional-integrating servo (PI-servo) with

$$G(s) = k_p + \frac{k_i}{s}.$$ (5.5)

A design of a servo circuit can be found in appendix B. Figure 5.2 shows the reaction of the system with and without regulation when the input signal jumps from zero to one as well as the reaction on perturbations.
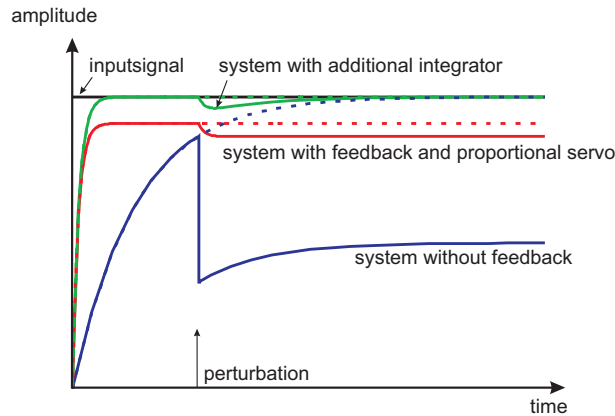
Figure 5.2: Reaction of a 1st order low pass to a step function as input signal with and without feedback. Dashed lines indicate the behavior without a perturbation. With a P-servo the system reacts faster but never reaches the full output amplitude. A PI servo is fast and able to cancel perturbations.

A P-servo provides a faster response than the system alone and has the ability to partially cancel perturbations. This can be seen in Figure 5.2. If k_p would be increased the cancellation of perturbations would be more efficient and the difference in the output amplitude would be decreased.

If a PI-servo is used, the output signal immediately reaches the full amplitude and perturbations are completely canceled.

The bigger k_p and k_i are, the faster is the system and the better it can compensate perturbations. At a first glance one might be tempted to make these values as big as possible to get the best performance. However one usually deals with systems of higher order which are able to change the phase by more than π which results in a change in sign in the denominator of the transfer function. At a certain frequency the negative feedback will change into positive feedback and the denominator can then even become zero. This happens when $S(s) \cdot G(s) = -1$ and the system will oscillate at this frequency s = i ω_{res}. So at high frequencies corrections are applied with the wrong phase which increases the perturbations. If an integrator is part of the servo the system might oscillate even easier because it adds a phase lag. A closer look into that is taken in the next chapter.

5.1.2 Servo-design for a 2nd order system

Now a 2nd order system with a resonance will be investigated. This system describes quite well the behavior of a piezo attached to a mirror which is used inside lasers to stabilize the cavity length. Its transfer function is given by

$$S(s) = \frac{\omega_0^2}{\omega_0^2 + \frac{\omega_0}{Q} s + s^2}. \tag{5.6}$$

Here ω_0 is the resonance frequency and Q is the damping factor of the resonance. The points where the phase equals 180° and the gain crosses unity gain are of

critical importance. Whether a system oscillates can be determined by looking at the open loop gain $S(s) \cdot G(s)$. Figure 5.3 shows a servo design, using again a P and a PI servo, with badly chosen parameters just to illustrate the problem.
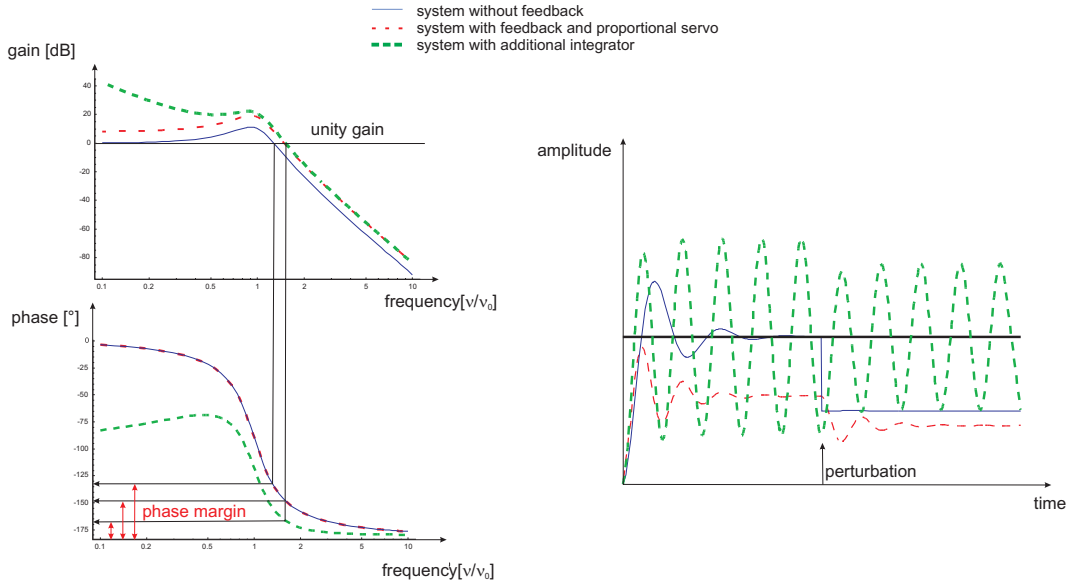

Figure 5.3: Left plot: open loop gain of the pure 2nd order system, system + P-servo and system + PI servo. Right plot: reaction of the three different systems to a step function at the input. The parameters for the servos are chosen such that the systems will start to oscillate.

The arrows in Figure 5.3 mark the phase of the open loop transfer function when the gain equals one. If the phase is 180° at that point, the system will oscillate with this frequency. Even if the phase is a little smaller, the system tends to be unstable and perturbations could make it ring. Therefore the phase margin should be at least 30°. One can see that the values for k_p and k_i cannot be increased arbitrarily because the system with the proportional servo is already at the limit. A bigger k_p would shift the curve further to the right and therefore reduce the phase margin. Additionally the servo did not improve the system's reaction on perturbations, it even got worse. The system with the integrator is already in the unstable regime very near to -180°. In the right part of Figure 5.3 oscillations caused by the additional phase lag of the integrator can be seen. Of course one can design the servo such that the ringing is minimized but then the performance won't be satisfactory.

The perturbations one has to deal with when stabilizing lasers, are mostly large excursions at low frequencies produced by acoustic noise and thermal drifts. This means that high gain in the low frequency regime is required to get rid of these perturbations. The example above suggested to do the opposite in order to get a stable system. At a first glance it seems one is stuck here, but there are ways around it.

The first idea is to add a derivative part to the controller to get a so called PID servo (proportional-integrating-derivative) with a transfer function

$$G(s) = k_p + \frac{k_i}{s} + k_p s. \tag{5.7}$$

The D-part of the controller adds a leading phase which can compensate the phase lag of the resonance. This controller can be optimized in such a way that it is capable of a fast and smooth settling by increasing the servo bandwidth. The increased bandwidth makes it possible to use higher gain values. Nevertheless the gain at low frequencies has not increased as much as one would wish. A better approach is to add a notch filter (band-stop filter) to the PI, which cancels exactly the resonance. Then, one can increase the gain especially at low frequencies but maintain unity gain at high frequencies. In practice one can even go a step further and add another PI stage or even several of them for even higher gain. Figure 5.4 shows the behavior of a double PI + notch and a PID + PI servo.
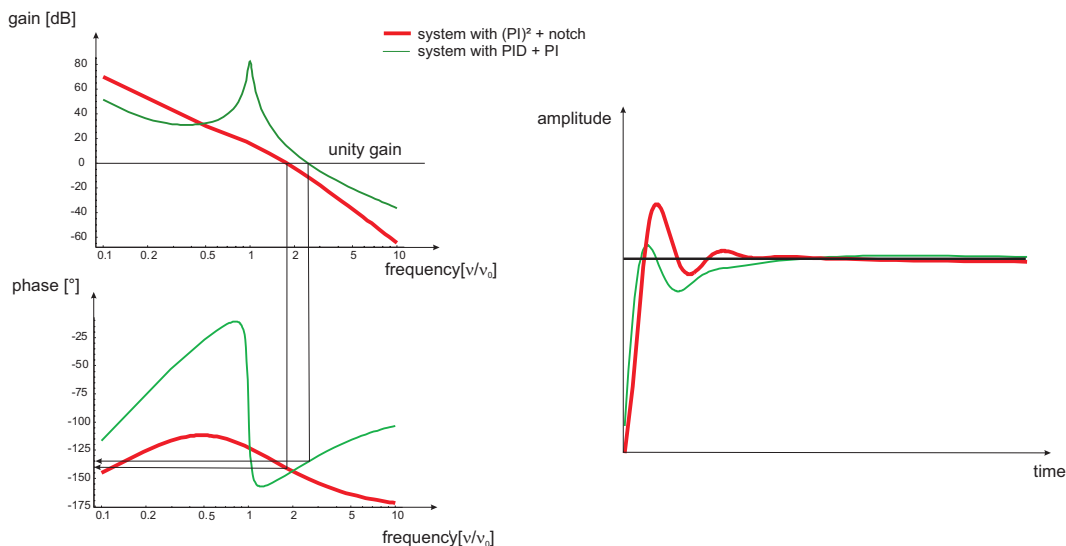

Figure 5.4: Improved systems with stable performance and high low frequency gain. Left plot: open loop gain of the system with PID + PI-servo and system with double PI servo + notch filter. Right plot: reaction of the two systems to a step function at the input.

Figure 5.4 shows that the low frequency gain has been improved by more than 30 dB for the double PI + notch servo (compare with Figure 5.3). Still, a stable system is maintained as can be seen in the response to a step function. The ringing is only minimal and the response is fast. The PID + PI servo does a comparable job but the gain at low frequencies is roughly 20 dB less. This means that the PI + notch servo can cancel low frequency perturbations better than the PID + PI servo. In practice it turns out that always at least two PI stages and a notch are used to achieve a tight and stable lock.

5.1.3   Rule of thumb for the servo design

There are several different methods for optimizing a servo to a system with a well known transfer function. These methods won't be described here but instead a method will be explained which can be applied in practice for systems that do not get harmed when reaching the stability boundary.

First one uses the P-term of the servo and increases it till the system starts oscillating. Then one measures the oscillation period T_{crit} and the gain k_{crit} of the servo. The servo parameters of equation 5.7 can then be calculated by the so called Ziegler Nichols method (see ref. [33]) which is based on experience.

Ziegler Nichols			
type of servo	k_p	k_i	k_d
PI	0.45 k_{crit}	$\frac{k_p}{T_{crit}}$ 0.32	
PID	0.6 k_{crit}	$\frac{k_p}{T_{crit}}$ 0.32	0.79 $k_p T_{crit}$

These values are just good starting points. One can experiment with them by either increasing them to get a tighter lock or lowering them for a more stable performance. If one wants to use a second PI stage it should be designed with a gain equal to one and a k_i with the same value as the first stage or up to ten times smaller. The choice of the k_i depends on whether one wants the most smooth settling or the highest possible low frequency gain.

5.2   Pound-Drever-Hall stabilization of a laser

The method used here to stabilize a laser was invented in the group of John Hall [7]. If compared to other locking schemes [36] [37] it has the big advantages that the locking range can be chosen to be very big and is independent of the very steep zero crossing. To create the PDH error signal one phase modulates a laserbeam to get sidebands, sends it to the cavity and detects the reflected signal. The setup is shown in Figure 5.5 where the EOM creates the sidebands and the reflected signal is detected on a photodiode with the help of a polarizing beamsplitter and a $\lambda/4$ plate. The photodiode detects the beatsignal of the carrier with the sidebands. The phase of these signals relative to each other depends on the detuning from the resonance of the cavity. With the help of a mixer this phase is detected and the signal is fed back onto the laser. In the following, the shape of the error signal will be derived following the references [38] and [39].

5.2.1   Theoretical description

When the beam has passed the EOM its electric field is phase modulated with the frequency Ω

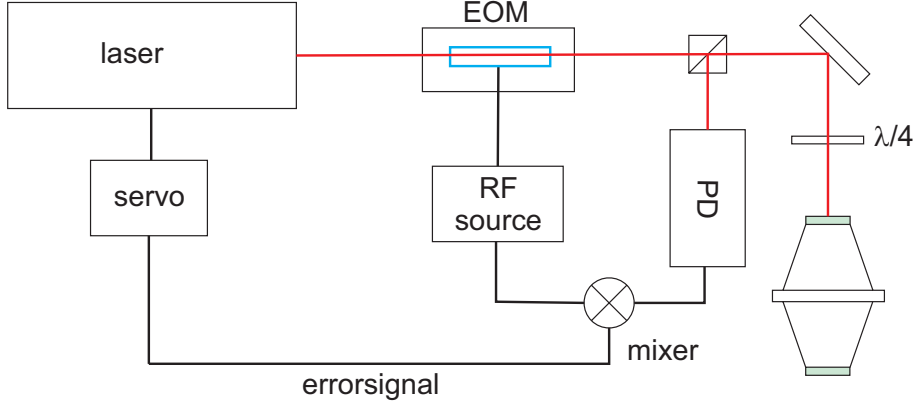$$E = E_0 \, e^{i(\omega t + \beta \sin(\Omega t))} \tag{5.8}$$

Figure 5.5: Setup for stabilizing a laser with PDH. The EOM creates sidebands on the light. The phododiode detects the beat between the reflected carrier and the sidebands. The beat is mixed to DC and the thereby created error signal is fed back to the laser

with the modulation index β. One can expand this expression using the Bessel-functions

$$E \approx E_0 \left(J_0(\beta)e^{i\omega t} + J_1(\beta)e^{i(\omega+\Omega)t} - J_1(\beta)e^{i(\omega-\Omega)t} \right). \tag{5.9}$$

This holds for $\beta \ll 1$. In this case almost all of the power is in the carrier and the sidebands are small. The phase modulated light is sent into the cavity and the reflection is measured. The reflection coefficient $F(\omega)$ is given by equations (3.3), (3.6) and (3.10)

$$F(\omega) = \frac{E_r}{E_i} = r\frac{e^{i\frac{\omega}{FSR}} - 1}{1 - r^2 e^{i\frac{\omega}{FSR}}} \tag{5.10}$$

The reflected wave is then given by

$$
\begin{aligned}
E_{ref} \;=\; & E_0\Big(F(\omega)J_0(\beta)e^{i\omega t} \tag{5.11}\\
+\; & F(\omega+\Omega)J_1(\beta)e^{i(\omega+\Omega)t}) - F(\omega-\Omega)J_1(\beta)e^{i(\omega-\Omega)t}\Big)
\end{aligned}
$$

The photodiode detects the power $P_{ref} = \mid E_{ref} \mid^2$ of the reflected beam. With the abbreviations

$$P_c = (E_0 \, J_0(\beta))^2, \quad P_s = (E_0 \, J_1(\beta))^2 \tag{5.12}$$

this leads to

$$
\begin{aligned}
P_{ref} \;=\; & P_c \mid F(\omega) \mid^2 + P_s \mid F(\omega+\Omega) \mid^2 + P_s \mid F(\omega-\Omega) \mid^2 \tag{5.13}\\
+\; & 2\sqrt{P_c P_s}\Big(\Re\{F(\omega)F^*(\omega+\Omega) - F^*(\omega)F(\omega-\Omega)\} \cos \Omega t \\
+\; & \Im\{F(\omega)F^*(\omega+\Omega) - F^*(\omega)F(\omega-\Omega)\} \sin \Omega t \Big) \\
+\; & (2\Omega \, \text{terms}).
\end{aligned}
$$

By adding up the carrier and the sidebands one gets a signal oscillating at ω with an envelope displaying a beat pattern with two frequencies. The Ω term arises from the interference between the carrier and the sidebands and the 2Ω terms are due to the sidebands interfering with each other. A mixer with a local oscillator (LO) operating at a frequency Ω extracts the terms with $\cos\Omega t$ or $\sin\Omega t$ dependening on the phase of the LO. The 2Ω terms are filtered by a lowpass.

In Figure 5.6 the error signal of equation (5.13) is plotted for two different phases of the local oscillator (LO), where the phase is defined relative to the $\sin\Omega t$ term. If the phase of the LO is set to $0°$ the slope of the zero crossing at the resonance of the cavity is maximal. One can see, that the zero crossings at the sideband frequencies Ω have the opposite sign and thus prevent locking to the sidebands. For this case the error signal is given by:

$$\epsilon = -2\sqrt{P_cP_s}\,\Im((F(\omega)F^*(\omega+\Omega) - F^*(\omega)F(\omega-\Omega))) \qquad (5.14)$$

The maxima of the desired error signal are located exactly at $\pm\frac{\Delta\nu}{2}$, so one can already guess that the slope is determined by the cavity linewidth. The sign of the slope at resonance can be conveniently chosen by changing the phase by π.
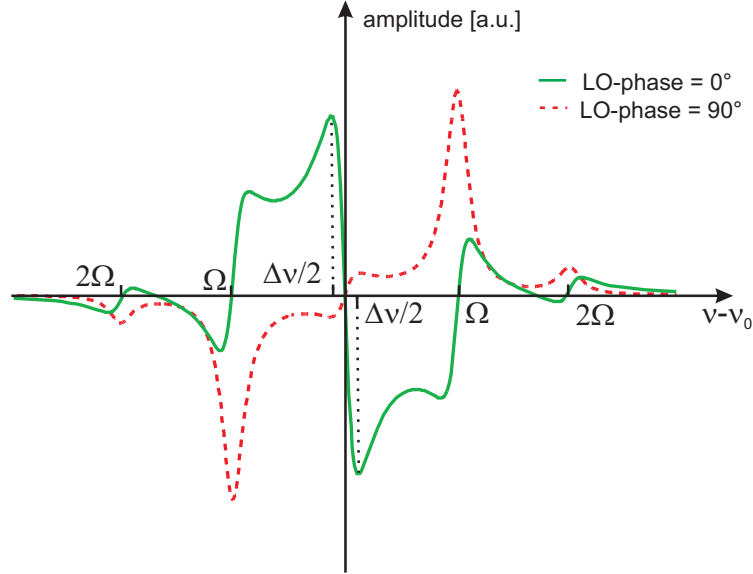

Figure 5.6: Calculated PDH error signal for two different phases of the local oscillator of the mixer. A LO phase of zero creates the desired signal with a steep slope at the zero crossing.

Before discussing how different parameters influence the slope of the error signal, Equation (5.14) will be simplified by making some assumptions.

If the light is in resonance with the cavity and the modulation frequency is higher than the cavity linewidth the sidebands are totally reflected. Then $F(\omega\pm\Omega) = -1$ and equation (5.14) reduces to

$$\epsilon = -4\sqrt{P_cP_s}\,\Im(F(\omega)). \qquad (5.15)$$

Near resonance one can write

$$\frac{\omega}{FSR} = 2\pi N + \frac{\delta\omega}{FSR} \tag{5.16}$$

where N is an integer and $\delta\omega$ is the deviation of the laser frequency from resonance. Additionally high reflectivity ($r \approx 1$) cavity mirrors are assumed so that equations (3.11), (5.10) simplify to

$$F(\omega) = i\frac{\delta\omega}{FSR}\frac{1}{1-r^2} \tag{5.17}$$

$$\mathcal{F} = \frac{\pi}{1-r^2} \tag{5.18}$$

By combining the upper two equations one gets

$$F(\omega) = i\frac{\delta\omega}{FSR}\frac{\mathcal{F}}{\pi} = \frac{i}{\pi}\frac{\delta\omega}{\Delta\nu}. \tag{5.19}$$

With this one can rewrite equation (5.15) and with $\delta\omega = 2\pi\,\delta f$ one obtains

$$\epsilon = -8\frac{\sqrt{P_c P_s}}{\Delta\nu}\delta f \tag{5.20}$$

The error signal is proportional to the frequency deviation of the laser from the resonance, where the slope is determined by the cavity linewidth and the power of the sidebands and carrier. Since a narrow linewidth is required for a good frequency discrimination a high finesse cavity is needed.

5.2.2 Maximizing the slope of the error signal

The steeper the slope of the error signal, the more sensitive it is to fluctuations of the laser frequency. To obtain a good stabilization of the laser, it has been shown that a large gain at low frequencies is needed. This can be achieved by increasing the slope of the error signal instead of amplifying it subsequently which would induce additional noise.

While the minimal linewidth of the cavity cannot be decreased arbitrarily, it is possible to optimize the modulation index β to get a maximal value for $\sqrt{P_c P_s}$. If this expression is written in terms of Bessel functions a maximum can be found at

$$\frac{P_s}{P_c} = 0.42 \tag{5.21}$$

resulting in an optimal modulation depth of $\beta = 1.08$ as shown in Figure 5.7.

If β is close to one, higher sidebands can't be neglected and contribute to the error signal (see Figure 5.6). Nevertheless, they do not change the slope at the center and therefore do not change the sensitivity. This can be by seen including more sidebands into the numerical calculation. Figure 5.8 shows the derivatives of the error signal calculated with one sideband and with two sidebands at $\beta = 1.08$. One can see, that the slope at the zero crossing is identical.

The slope of the error signal at the zero crossing is exactly twice the peak to peak voltage of the PDH signal over the cavity linewidth.
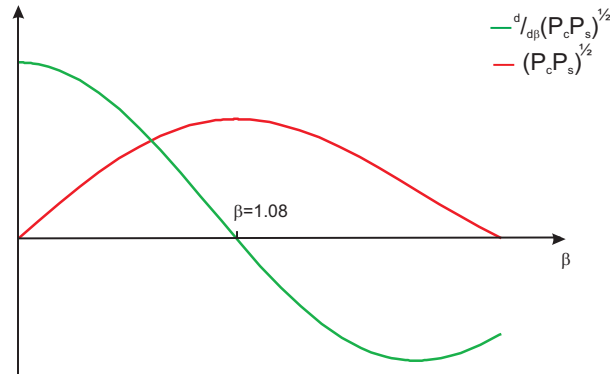
Figure 5.7: Dependence of $\sqrt{P_c P_s}$ and its derivative, on the modulation index β

5.2.3   Problems caused by an asymmetric error signal

The errorsignal of a purely phase modulated laser beam is zero when the laser is in resonance with the cavity mode. The carrier is completely transmitted and the two sidebands are reflected with a 180° phase and thus exactly cancel each other. Every perturbation of this symmetry causes an additional offset so that the zero crossing is off the resonance. This is even worse if the perturbations are time dependent.

Possible sources of perturbations creating an offset are the following:

- The polarization of the light does not match the crystal axis of the EOM. In this case, the polarization is rotated with the modulation frequency of the EOM. The subsequent polarizing beam splitter produces an amplitude modulation of the light and thus prevents a perfect cancellation of the sidebands at the photodiode. This produces a DC-offset after the mixer. Thus the polarization of the light has to be carefully aligned with the crystal axes. In this setup a Glan-Thompson polarizer (extinction ratio 10^{-6}) is used for a good polarization.

- It has been observed that an EOM is capable of producing residual amplitude modulation [40]. If the crystal is cut at Brewster angle internal backscattering is prevented and the residual modulation is minimized. Here a Linos PM25 EOM is used which has two Brewster cut crystals inside.

- Another problem is crosstalk between the signal modulating the EOM and the photodiode detecting the error signal. This again causes a DC-amplitude after the mixer. Shielding of the photodiode and reducing the stray fields of the RF helps to get rid of this problem.
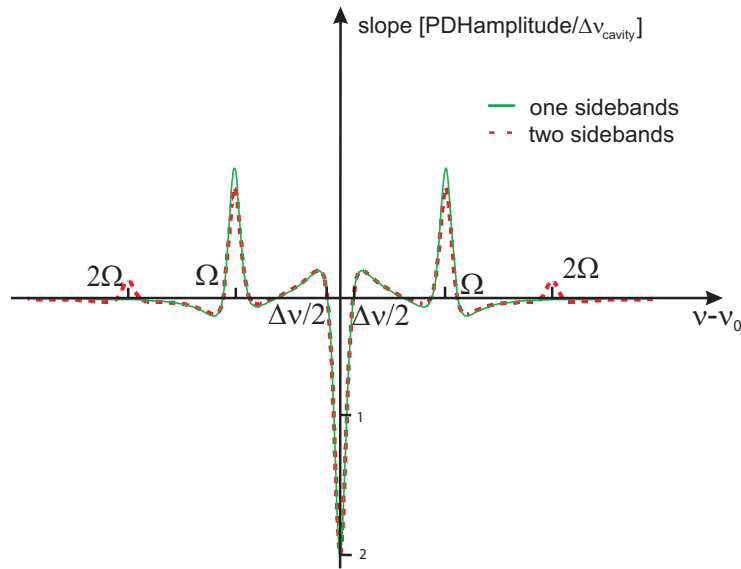
Figure 5.8: Derivative of error signal including 1 or 2 sidebands in the calculation. Y axis in units of PDH peak to peak voltage over cavity linewidth. The slope of the error signal is the same no matter if one or more sidebands are included in the calculation.

5.3 3-fold feedback on the 729 nm laser

There are several possibilities for applying a feedback onto a laser to stabilize its frequency. The most common one is a feedback onto piezos controlling the length of the laser resonator. This technique works for frequencies up to several kilohertz. It is limited by the resonances of the piezo which prevents compensation of fast disturbances. Therefore one has to think of an additional way of providing a feedback.

One possibility is to put an EOM inside the cavity of the laser resonator. By varying the refractive index of the crystal the length of the laser resonator can be kept constant. The advantage is that the servo loop bandwidth increases up to some MHz and the loss in output power is only about 10% when cutting the crystal at Brewster angle. The position of the EOM inside the laser is shown in Figure 2.2.

5.3.1 Feedback scheme

The error signal is fed back to the TiSa in the following way (see Figure 5.10):

- The laser is prestabilized with the Coherent locks to a linewidth of about 500 kHz.

- A slow feedback with a bandwidth of roughly 9 kHz is applied to the tweeter and the scanning Brewster plate. It is not directly sent to these elements but rather fed to the Coherent electronics. This is done by adding the correction to the signal coming out of the differential amplifier

on board 1A9 of the Coherent electronics, which is indicated in Figure 2.6 by the adder. The signal is then sent over a PI stage and a high voltage amplifier in the Coherent box onto the tweeter and the Brewster plate. Additionally, there are notch filters implemented just before the tweeter and the Brewster plate to suppress their resonances.

- A mid-frequency feedback is done by a high voltage (HV) amplifier capable of dealing with voltages up to 400V and frequencies up to 800 kHz. It is connected to one electrode of the EOM.

- The ground of the HV amplifier is connected to the ground of a fast small signal amplifier[1] which supplies its feedback to the other electrode of the EOM. This commercial amplifier has a bandwidth of 10 MHz and can create output amplitudes of ±15V at high ohmic loads. It has a constant gain which is adjusted to the needed value by adding attenuators at the input.
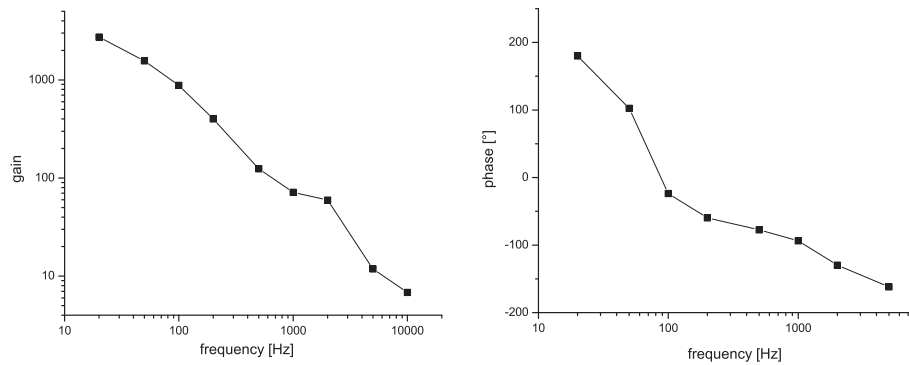

Figure 5.9: Transfer function of the coherent system used for the feedback onto the piezo and Brewster plate. The slope of the curve is roughly -10 dB/decade at frequencies below 100 Hz and increases to about -20 dB/decade above.

The EOM has a $\lambda/10$ voltage of 200 V. Together with the free spectral range of the laser resonator of roughly 150 MHz, this implies that 1 V at the EOM changes the frequency of the laser by 75 kHz. The 3 dB bandwidth of the EOM is specified to 10 MHz which is sufficient for this purpose. The piezo changes the frequency of the laser by 1.1 MHz/V but has a bandwidth of only 10 kHz.

The transfer function of the Coherent system used for the feedback, behaves like an integrator for frequencies up to 10 kHz (Figure 5.9). The measurement of this transfer function is not that easy, because one can not separate this part from the rest of the box. The piezo can not be unplugged completely because the high voltage stage of the circuit would be damaged. The transfer function was measured by putting a resistor cascade with a total resistance of 20 MΩ in parallel to the piezo. Then one fifth of the output voltage was measured with

---

[1]Femto HVA-10M-60-F

part	gain	bandwidth	integrator frequency
PI-piezo	2.5	3 MHz	7.2 kHz
PI-HV	10.5	800 kHz	23.4 kHz
HV Amplifier	26.5	800 kHz	none
fast Amplifier & attenuators	124	10 MHz	none

Table 5.1: Servo parameters for the TiSa lock.

an oscilloscope. Additionally the transfer function of the cascade was measured to obtain the true transfer function of the system.

The servos for the piezo and the high voltage part are PI stages. The high frequency part is a pure proportional servo. The feedback on the piezos is additionally sent over the PI stages inside the Coherent box. This effectively leads to a double PI stage. An additional third PI in this branch would increase the low frequency gain further. Nevertheless it was not implemented because it made the system unstable.

The incident light power on the cavity was about 40 μW to minimize heating of the cavity mirrors. The expected change in frequency due to mirror heating is roughly 1 Hz/μW [5]. The amplitude of the PDH signal was roughly 840 mV peak to peak with a sideband height of 15 % of the carrier. This corresponds to a modulation index of about 0.6. With this value the slope of the error signal is 20 % below the optimum (see chapter 5.2), but no bigger sidebands could be produced with this EOM to go to the optimal point.

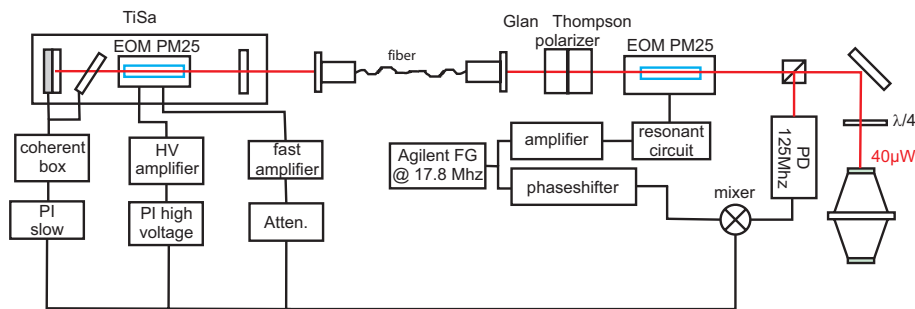Figure 5.10 shows the locking scheme.

Figure 5.10: Lock setup. The feedback to the TiSa is threefold. A slow feeback is applied to the tweeter and the Brewster plate. A mid and a high frequency feedback is applied to an intracavity EOM.

The parameters used for the PI stages and the amplifiers are shown in table 5.1. The measured Bode plots and the circuit layouts can be found in appendix B.

The integrator of the HV part was limited to a constant gain below 100 Hz to avoid a competition between the two integrators at DC. Without that precaution, a situation might occur where the integrators compensate each other and

run off in different directions until they reach their limit and the laser falls out of the lock. When the feedback loop is closed the laser stays in lock for several hours (up to 12 h), mostly until someone bangs on the table.

5.3.2   In-loop error signal

When the laser is locked to the cavity, one can optimize the three feedback parts by looking at the noise spectrum of the in-loop error signal. One can get some hints at which frequencies problems occur. Though one has to be careful not to look at signals created by some RF stray fields.

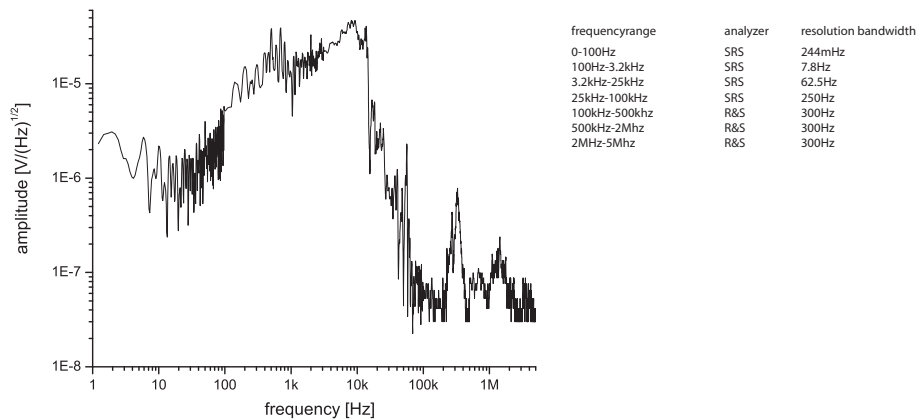| frequencyrange	analyzer	resolution bandwidth
0-100Hz	SRS	244mHz
100Hz-3.2kHz	SRS	7.8Hz
3.2kHz-25kHz	SRS	62.5Hz
25kHz-100kHz	SRS	250Hz
100kHz-500khz	R&S	300Hz
500kHz-2Mhz	R&S	300Hz
2MHz-5Mhz	R&S	300Hz

Figure 5.11: Fast Fourier transform of the in-loop error signal for the laser lock. Servo bumps can be seen at 8 kHz for the piezo stage, at 250 kHz for the HV stage and at 1.4 MHz for the fast amplifier stage.

The spectrum was measured with a FFT-analyzer from 0 to 100 kHz and with a spectrum-analyzer from 100 kHz to 5 MHz. The signal is given in units of $V/\sqrt{Hz}$ because one cannot set the resolution bandwidth independent from the span in the FFT analyzer. The signal plotted in Figure 5.11 consists of seven measurements combined in one graph with the ranges and resolution bandwidth listed in the plot. An averaging has been done over ten measurements each.

   Figure 5.11 shows certain structures related to the lock. The peak around 8 kHz corresponds to the point where the phase of the feedback signal for the piezo passes 180°. This is a so called servo bump. The peak at 250 kHz is created by the HV amplifier feedback and the resonance at 1.4 MHz is the high frequency part. By looking at the Fourier spectrum, the three parts of the lock can be optimized. We desire a high gain and thus a stable locking without too pronounced servo bumps. In this graph one can also see that the main problems of the feedback loop are in the few kHz regime. Especially the pedestal like structure around 10 kHz could cause problems. This step in the error signal occurs at frequencies where the overall gain of the feedback drops due to the limited bandwidth of the piezo. The overall gain vs. frequency can be seen in Plot 5.12. One could possibly get rid of this step by substituting the Coherent lock box by a system designed especially for locking the laser.

Perhaps even a change of the piezo and mirror inside the TiSa, to get a higher servo bandwidth, would be necessary. Nevertheless we will see that the lock is not the yet the limiting factor (see chapter 6.1.2) in the laser setup.
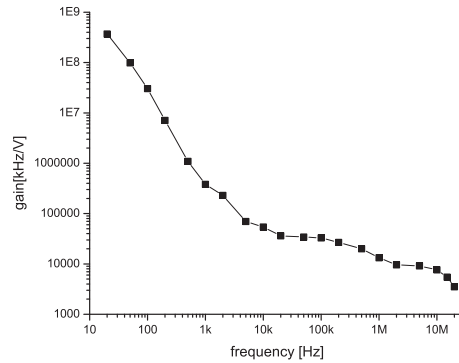

Figure 5.12: Overall gain of the feedback onto the laser. The high gain at low frequencies is produced by the piezo stage, whereas the tail above ten kHz is due to the HV amplifier and the fast amplifier

The gain in Figure 5.12 is given in units kHz/V. One volt applied at the input of the servo changes the laser frequency by that amount. The scaling was done by knowing how the frequency of the laser changes when a voltage is applied on the EOM or the piezo.

Chapter 6

Laser linewidth

We want to determine the performance of the laser locked to the cavity. The linewidth of the laser can be measured by beating it with another comparable laser or by a measurement on a narrow atomic transition. Furthermore it is possible to quantify the tightness of the lock to the cavity by looking at the in-loop error signal.

6.1 Performance estimation with the in-loop error signal

6.1.1 Theoretical description

When the laser is in lock, the error signal is a good measure for the quality of the lock to the cavity. However, it is not completely straightforward to determine the laser-linewidth from the error signal. With the help of the autocorrelation function one is able to calculate it. Here just the basic idea will be explained, more information can be found in a paper by D. S. Elliott et.al. [41].

An infinitely narrow laser is assumed in this derivation which will be broadened with an AOM driven by a voltage controlled oscillator (VCO). The VCO is fed by a noise source with a Gaussian probability distribution in a certain bandwidth. The output signal of the oscillator is of the form

$$V_f(t) = A_0 \, e^{i[\omega_0 t + \Phi(t)]} \tag{6.1}$$

and

$$\Phi(t) = 2\pi \int_0^t DV(t')dt' \tag{6.2}$$

where one assumes that $\Phi(t)$ is a Gaussian process since V(t') is a Gaussian process. The slope of the tuning curve of the VCO is denoted with D and ω_0 is the central frequency. One has to calculate now the RF power spectrum created by the frequency modulation to obtain the laser linewidth. For that

the autocorrelation function $R_f(\tau)$ of $V_f(t)$ has to be determined

$$R_f(\tau) \quad = \quad \frac{1}{2}Re\Big\{ \lim_{T \to \infty} \frac{1}{T} \int_{-T/2}^{T/2} V_f(t)V_f^*(t+\tau)dt \Big\} = \qquad (6.3)$$

$$= \quad \frac{1}{2} < V_f(t)V_f^*(t+\tau) >= \qquad (6.4)$$

$$= \quad \frac{A_0^2}{2} \cos(\omega_0 \tau)e^{-1/2<[\Phi(t)-\Phi(t+\tau)]^2>} \qquad (6.5)$$

Now one can apply the Wiener-Khintchine Theorem to relate the power spectrum $W(f)$ and the autocorrelation function

$$W(f) \quad = \quad 4 \int_0^\infty R(t) \cos(\omega t)dt \qquad (6.6)$$

and

$$R(t) \quad = \quad \int_0^\infty W(f) \cos(\omega t)df \qquad (6.7)$$

to get

$$W_f(f) = A_0^2 \int_0^\infty d\tau [\cos(\{\omega_0 - \omega\}\tau) + \cos(\{\omega_0 + \omega\}\tau)]e^{-1/2<[\Phi(t)-\Phi(t+\tau)]^2>} (6.8)$$

where the rapidly varying term $\cos(\{\omega_0 - \omega\}\tau)$ can be ignored. Now the argument of the exponential function has to be evaluated, which can be done for this specific application. It can be shown that

$$< [\Phi(t) - \Phi(t+\tau)]^2 >= 2(2\pi D)^2 \int_0^\infty dt(\tau - t)R_v(t) \qquad (6.9)$$

with $R_v(t)$ the autocorrelation function of the noise applied to the VCO. Using again the Wiener-Khintchine Theorem the power spectrum of the laser is

$$W_f(\Delta\omega) \quad = \quad \frac{A_0^2}{2\pi} \int_0^\infty d\tau \, \cos(\Delta\omega\,\tau)$$

$$\exp\Big[- 8(\pi D)^2 \int_0^\infty W_v(\omega')\Big(\frac{\sin(\omega'\tau/2)}{\omega'}\Big)^2 d\omega' \Big] \qquad (6.10)$$

with $\Delta\omega = \omega - \omega_0$ and $W_v(\omega')$ the power spectrum of the noise. Now consider the case of a rectangular input noise power spectrum with a cut-off at frequency B and an amplitude of V_{rms}^2

$$W_v(\omega) = \begin{cases} \frac{V_{rms}^2}{2\pi B} \, , 0 < \omega < 2\pi B \\ \quad 0 \, , \omega > 2\pi B \end{cases} \qquad (6.11)$$

which leads to a laser power spectrum of

$$W_f(\Delta\omega) = \frac{A_0^2}{2\pi} \int_0^\infty d\tau \, \cos(\Delta\omega\,\tau) \, \exp\Big[- \frac{2\pi D^2 V_{rms}^2 \tau}{B} \int_0^{\pi B\tau} \Big(\frac{\sin x}{x}\Big)^2 dx \Big] (6.12)$$

Equation (6.12) shows that higher frequencies do not contribute much because of the $\left(\frac{sinx}{x}\right)^2$ term which is an important fact when calculating the linewidth of the laser.

In the case of a well stabilized laser the ratio of deviation frequency to cutoff frequency DV_{rms}/B is small. Thus one can approximate the integral

$$\int_0^{\pi B\tau} \left(\frac{\sin x}{x}\right)^2 dx \tag{6.13}$$

by its asymptotic value of $\pi/2$. After calculating the outer integral the power spectrum is

$$W_f(\Delta\omega) = \frac{A_0^2}{2\pi} \frac{\pi^2 D^2 V_{rms}^2/B}{(\pi^2 D^2 V_{rms}^2/B)^2 + (\Delta\omega)^2} \tag{6.14}$$

which is a Lorentzian power spectrum with a full width half maximum of

$$FWHM = \frac{\pi D^2 V_{rms}^2}{B} \tag{6.15}$$

In this case, the laser linewidth is simply proportional to the RMS value of V.

6.1.2 Calculation of the locking performance

Equation (6.15) can now be translated to the problem of determining the lock to the cavity. The slope of the VCO will be replaced by the slope of the PDH signal at the zero crossing. The bandwidth of the noise will be determined with two different approaches. In the first approach we assume, that the cavity dictates the bandwidth and the noise V_{rms} will be measured with an oscilloscope.

The second approach uses the measured in loop error signal. In Figure 5.11 it can be seen, that the main part of the noise occurs in a bandwidth of 10 kHz so we can assume a rectangular noise spectrum from zero to 10 kHz. The average amplitude of the noise is calculated by integrating over the measured spectrum from 0 to 10 kHz. In the calculation the amplitudes were corrected for the low pass characteristics of the cavity.

The assumption the cavity dictates the bandwidth respectively the noise bandwidth is 10 kHz (see figure 5.11) is valid due to the following reason. Higher frequencies in the fourier spectrum of the error signal do not contribute much to the linewidth (see chapter 6.1.1). As the error signal has less noise in frequencies below 100 Hz the following calculation is most likely just an upper limit.

The slope of the PDH can be easily deduced by looking at the peak to peak value of the error signal and dividing it by the cavity linewidth times a factor of two (see chapter 5.2.2). Only the non-linearity of the mixer has to be taken into account (see appendix C) for measuring the peak to peak voltage of the PDH signal. A similar calculation for the locking performance to the cavity can be found in a paper by John Hall [6].

The values for the first approach, where the cavity is the bandwidth determining element, are the following

$$
\begin{aligned}
V_{rms} &= 8\,mV \pm 2\,mV \\
B &= 2349\,Hz \pm 2\,Hz \\
D &= 2.8\,Hz/mV \pm 0.3\,Hz/mV
\end{aligned}
$$

These values lead to a linewidth of the laser relative to the cavity of

$$
\Delta\nu = 0.67\,Hz \pm 0.37\,Hz
$$

The values for the second approach using the spectrum of the error signal

$$
\begin{aligned}
V_{rms} &= 15\,mV \pm 2\,mV \\
B &= 10\,kHz \pm 100\,Hz \\
D &= 2.8\,Hz/mV \pm 0.3\,Hz/mV
\end{aligned}
$$

result in a linewidth of

$$
\Delta\nu = 0.56\,Hz \pm 0.51\,Hz
$$

These results show that the lock to the cavity is tight and should not be the limiting factor. Similar values were published in a paper on a sub Hertz linewidth laser from NPL [5].

6.2 Beat measurement of the two 729 nm lasers

One approach of measuring the short term stability of a laser is to use a Fabry Perot that has a linewidth equal to the one used for laser stabilization. At the moment no second high finesse cavity is available so a different method has to be found. Another technique relies on the measurement of a beat between two similar lasers at a difference frequency in the RF regime so that counting or a FFT analysis is possible.

6.2.1 Theoretical description

The beat signal can be described by

$$
I(t) = |E_1(t) + E_2(t)|^2 = |E_1(t)|^2 + |E_2(t)|^2 + 2Re\{E_1(t)^*E_2(t)\} \quad (6.16)
$$

where the part containing information about the linewidth is the interference term. For two lasers it is equal to

$$
E_1(t)^*E_2(t) \propto e^{i\delta\omega t}e^{i\delta\Phi(t)} \quad\quad (6.17)
$$

with a difference frequency of $\delta\omega = \omega_1 - \omega_2$ and difference phase $\delta\Phi = \Phi_1 - \Phi_2$. Thus the beat is directly related to the difference frequency and its fluctuations. Again one wants to determine the spectrum of this beat by calculating the

autocorrelation function. After some calculation (see [41], [42]) one can get the
following autocorrelation function

$$R_{E_1^* E_2}(\tau) \propto e^{i\delta\omega\tau} e^{-\frac{1}{2}<[\delta\Phi(t)-\delta\Phi(t+\tau)]^2>} \tag{6.18}$$

If the assumption that both laser fluctuations obey they same statistics but are
independent of another holds, so that

$$R_{\Phi_1^* \Phi_2}(\tau) \propto < \Phi_1(t)\Phi_2(t+\tau) >= 0 \tag{6.19}$$

one can rewrite equation (6.18)

$$R_{E_1^* E_2}(\tau) \propto e^{i\delta\omega\tau} e^{-\frac{1}{2}<[\Phi_1(t)-\Phi_1(t+\tau)]^2>+<[\Phi_2(t)-\Phi_2(t+\tau)]^2>} = R_{E_1^*}(\tau)R_{E_2}(\tau) \tag{6.20}$$

If the Wiener Kintchin theorem is applied, one can see that the power spectrum
of the beat is the convolution of the power spectra of the lasers

$$W_{E_1^* E_2}(f) = W_{E_1^*}(f) \otimes W_{E_2}(f) \tag{6.21}$$

If the lasers are dominated by white noise they have Lorentzian spectra and
the beat is again Lorentzian with a FWHM being the sum of the individual
linewidth.

If the lasers are dominated by $\frac{1}{f}$ noise one gets a Gaussian spectrum where
the FWHM add up as $\sqrt{\Delta\nu_1^2 + \Delta\nu_2^2}$.

6.2.2 Results of the beat measurement

Two independent TiSa lasers stabilized on cavities of the same type with two
similar locking schemes were compard with each other. The lasers were 500
m apart connected via a fiber where the fiber noise was canceled to prevent
a broadening of the spectra. The beat was measured on a photodiode and
recorded with the FFT analyzer and the spectrumanalyzer.

First a bigger span was chosen, to see if the structures which can be seen
in the in-loop error signal can also be seen in the beat note. In the left part of
Figure 6.1 a spectrum is shown spanning 5 MHz. No structures related to the
high frequency or the HV servo bump can be seen even 50 dB below the carrier.
The right part of Figure 6.1 shows the spectrum closer to the beat frequency
in higher resolution. One can clearly see some features which can be identified
in the in-loop error signal of the lasers. The pedestal marked with the arrow is
most probably from the $^{43}Ca^+$ TiSa. It fits well with the pedestal seen in the
error signal. The peaks and spikes are not related to this laser but some similar
structures can be seen in the error signal of the $^{40}Ca^+$ TiSa.

Then the beat was shifted to around 60 kHz to measure it with the FFT
analyzer to get a better resolution. This time the measured data are plotted on
a linear scale to determine the FWHM. The measurement time was 2 seconds
and a Lorentzian fit was applied to the data, which matched better than a
Gaussian fit. The linear drift of about 2.5 Hz/s, of the cavities relative to
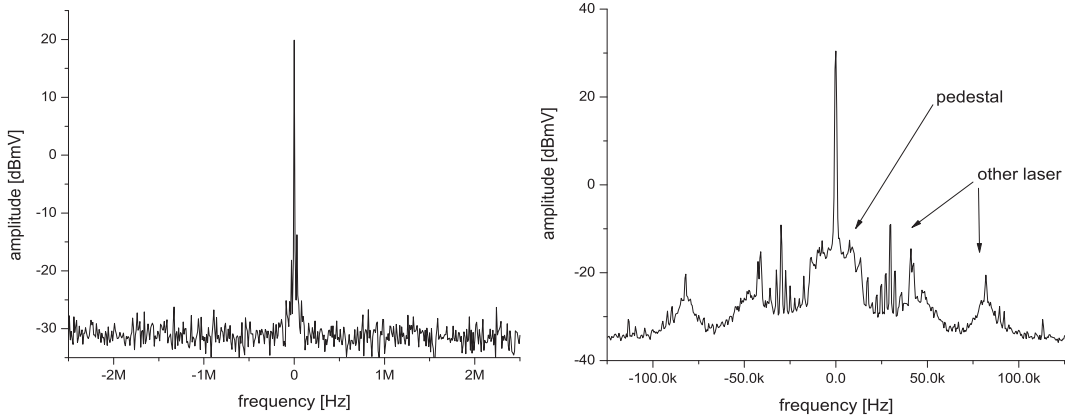another, was compensated by an AOM.

Figure 6.1: Beat of two TiSa lasers measured with a spectrum analyzer. Frequencies relative to beat center frequency. In the right plot features related to the lock can be seen in the beat. These structures are more than 40 dB below the carrier.

The resulting FWHM of a Lorentzian fit to the data is

$$\Delta\nu = 3.4\,Hz \pm 0.1\,Hz \tag{6.22}$$

which would lead to a linewidth of a single laser[1] in a measurement time of 2 seconds of

$$\Delta\nu = 1.7\,Hz \pm 0.1\,Hz.$$

This result fulfills the requirement of a linewidth below 10 Hz. It also demonstrates that the lock to the cavity is not yet the limit because it is a factor of two better (chapter 6.1.2) than the linewidth measured here.

The problem with the laser lock is, that every acoustic noise or vibration in one of the two labs could be seen clearly in the beat. The beat was not always as narrow as in Figure 6.2 but rather getting much broader due to the noise. The measurement will be repeated when the labs are quiet and disturbances are minimal to see a convincing and stable result.

The main noise sources in this lab are the Verdi power supply and the air condition system. In the future their noise will be reduced by some acoustic shielding.

Problems in the setup could be characterized by using a very steep filter. If the beat signal coincides with the flank of this filter one could see the frequencies causing the broadening of the beat. Then the origin of these perturbations might be found. At the moment no such filter is available.

Another measurement was done for an averaging time of 10 seconds where the result was a linewidth for each laser of roughly 20 Hz again dominated by noise in the lab and some uncompensated drifts.

---

[1]For a Lorentzian lineshape the total width of the beat is the sum of the individual linewidth.
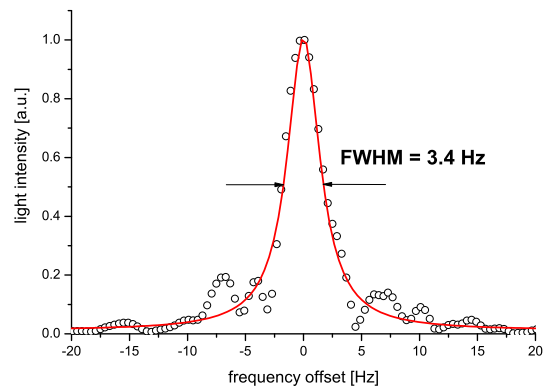
Figure 6.2: Beat of two TiSa lasers measured with a FFT analyzer. Resolution bandwidth = 0.488 Hz. The FWHM of the beat is only 3.4 Hz which leads to a linewidth of a single laser of 1.7 Hz.

Chapter 7

Spectroscopy of $^{40}Ca^+$

The laser has been implemented into the quantum information experiment with $^{40}Ca^+$ and $^{43}Ca^+$. In this chapter spectra of the $S_{1/2}$ to $D_{5/2}$ transition and Rabi oscillations on the carrier transition will be shown.

7.1 Spectroscopy of the quadrupole transition of $^{40}Ca^+$
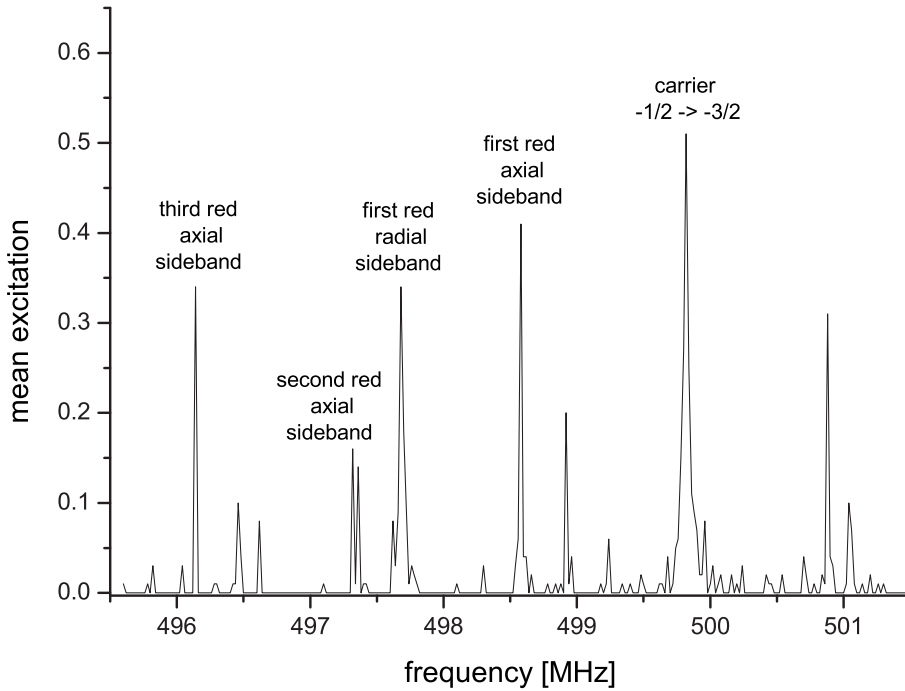

Figure 7.1: Spectrum in the vicinity of the $S_{1/2}$, $m_f = -1/2$ to $D_{5/2}$, $m_f = -3/2$ transition of $^{40}Ca^+$. Radial and axial sidebands as well as the carrier can be seen.

The procedure to measure an excitation spectrum of the $S_{1/2}$ to $D_{5/2}$ quadrupole transition is the following: With Doppler cooling and optical pumping the ion is

prepared in $S_{1/2}, m_f = -1/2$. Then the 729 nm laser is switched on for a short time, followed by a detection of the state. If the laser was in resonance with a transition the ion was excited to the $D_{5/2}$ state. Now the ion will not scatter any photons when excited on the $S_{1/2}$ to $P_{1/2}$ transition. This procedure is repeated 100 times for one frequency of the 729 nm laser to get a better statistics. After this the frequency is changed and the sequence starts from the beginning. A typical spectrum can be seen in Figure 7.1 with the carrier transition being the highest line. Also clearly visible are the axial and radial sidebands, 1.4 MHz and 2.3 MHz away from the carrier. This measurement was done with a 10 kHz resolution and 100 repetitions per point.

The carrier transition was then resolved with a 100 Hz step size, which can be seen in plot 7.2. The resulting linewidth of 900 Hz is much higher than the natural linewidth of 0.16 Hz. One reason for the increased linewidth is that the light sent onto the ion is broadened by the guiding fiber. A fiber noise cancellation can not be implemented in the current setup, because the light is switched before the fiber. Also fluctuations of the magnetic field add to the linewidth of the measured transition. The biggest parts of the magnetic field fluctuations are caused by 50 Hz noise and can usually be suppressed by line-triggering the experiment. This was not yet implemented when these measurements were done.
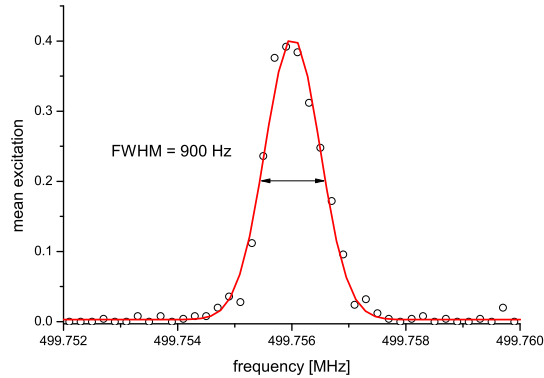

Figure 7.2: $S_{1/2}$, $m_f = -1/2$ to $D_{5/2}$, $m_f = -3/2$ transition of $^{40}Ca^+$ resolved with 100 Hz step size. Measured linewidth of this transition was 900 Hz. This is due to magnetic field fluctuations and a broadening of the light spectrum by the fiber.

7.2 Rabi oscillations on the quadrupole transition of $^{40}Ca^+$

The sequence for recording the Rabi flops is quite similar to the one described in the previous section. The ion is again prepared by Doppler cooling and optical pumping. The 729 nm laser is tuned to the resonance of the $S_{1/2}$, $m_f = -1/2$

to $D_{5/2}$, $m_f = -5/2$ transition. The laser is then switched on for a certain time followed by a detection of the state of the ion. This experiment is repeated 100 times for the same excitation time of the laser. Then the excitation time is increased and the experiment is rerun. The Rabi oscillations recorded in that way are shown in Figure 7.3. The Rabi oscillations start with a contrast of 100% and decay quickly most probably due to magnetic field fluctuations and a too high ion temperature.
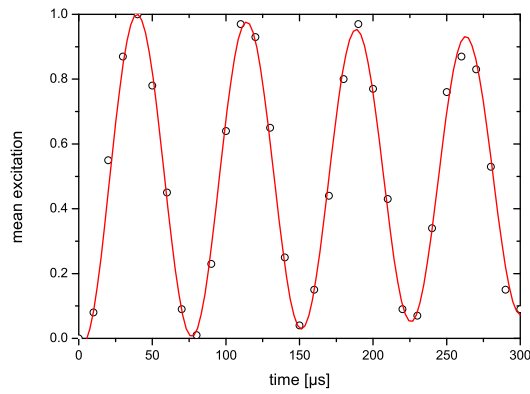

Figure 7.3: Rabi oscillations on the $S_{1/2}$, $m_f = -1/2$ to $D_{5/2}$, $m_f = -5/2$ transition of $^{40}Ca^+$. The decay is due to magnetic field fluctuations and a too high ion temperature.

Chapter 8

Conclusions and outlook

The goal of this diploma thesis was to build a laser with a few Hz linewidth and a stable locking performance for several hours.

The thesis started with an introduction to the $^{43}Ca^+$ experiment and an explanation of the purpose of the 729 nm laser. Then the basic functions and interior of a TiSa have been explained as well as the locking electronic that was supplied with it. Since this electronic is only capable of stabilizing the laser to a linewidth of 500 kHz it had to be modified to reach the desired laser linewidth. Amplitude noise spectra of TiSa and Verdi have been measured to see up to which frequencies an amplitude stabilization is necessary.

This was followed by a description and characterization of the cavity and the measurement of its parameters. The resulting finesse of 411540 confirmed the guaranteed specifications. Measures for temperature stabilizing the cavity and additional decoupling from the environment were explained. Especially the temperature stabilization has to be improved further so that variations over the day can not be seen and only a constant drift due to the cavity material remains. Longterm drifts in the order of 0.2 Hz/s have been observed. This would be good enough for the experiment but the problem was that this drift was not constant and variations on a 24 h cycle were observed. Thus a second stabilization stage was recently implemented inside the wooden box but so far no new measurements have been taken to quantify the effect.

After that the optical setup to generate the locking and the experimental beams was described. The setup was built such that the laser can be used for spectroscopy on $^{40}Ca^+$ and $^{43}Ca^+$. The principle of the fiber noise cancellation and the importance for the experiment were outlined. It was shown that even a 500 m long fiber can be stabilized such that it adds less than 1 Hz noise to the light.

Basic feedback theory and servo system design have been introduced. The derivation of the Pound-Drever-Hall error signal and how to set the parameters for a stable lock have been discussed. This part ended with the implementation and the design of the feedback loops and a short characterization of them. Especially the three-fold feedback presented in this chapter is the keystone to stabilize the laser to a linewidth below 10 Hz. The layouts of the circuits necessary to do the locking are shown in the appendix.

Then the quality of the servo loop was determined. The measurements show a linewidth relative to the cavity of about 0.7 Hz. The beat measurement of the two lasers allows us to set an upper boundary for the laser linewidth. The result was a 2 Hz linewidth in 1 second and around 20 Hz in 10 seconds averaging time. This result fulfills the requirements defined for the laser. So far one can conclude, that the linewidth of the laser is more than good enough for the purposes needed in the $^{43}Ca^+$ experiment. To get a real clock laser further investigations and improvements would have to be made. Especially all noise sources creating vibrations on the lab table have to be damped.

Measurements on the $^{40}Ca^+$ $S_{1/2}$, $m_f = -1/2$ to $D_{5/2}$, $m_f = -3/2$ transition have been performed. The spectra show the carrier as well as axial and radial sidebands. The carrier was then resolved with a 100 Hz step. This line had a width of 900 Hz broadened by magnetic field fluctuations and fiber noise effects.

Currently there are measurements running on $^{43}Ca^+$ where already spectra of the $S_{1/2}$ to $D_{5/2}$ transition have been recorded. These measurements also indicate a very low laser linewidth. An absolute determination of the linewidth of the laser is possible by measuring a magnetic field insensitive transition. A cesium fountain clock will be used to calibrate the frequencies of the quadrupole transition. The ion together with the laser and a frequency comb can then serve as a tool for determining the absolute frequency and stability of lasers in the lab.

Appendix A

TiSa

A.1 Changes in the Coherent electronic

The changes described in chapter 2.3 have to be made on the 1A1 print inside the Coherent box (see [23]). A switch was put in to change between internal and external 2 kHz operation. That means the circuit paths between R108 and CR3, CR4, R91 as well as A11 and R96 have to be interrupted and reconnected over the switch. The external 2 kHz signal should have an amplitude of 12 Vpp according to [23] but can be reduced to 10 Vpp. The thick etalon is still locked but the fluctuations in the output power are diminished.

The phase shifter/attenuator takes the signal from TP10 and adds it to the piezo branch on the A4 board Pin2. The adder circuit can be found in appendix B. The amplitude and phase have to be tuned carefully for an optimal 2 kHz suppression.

A.2 Tips and tricks for the TiSa operation

After working for some time with the TiSa, one learns some tricks helping in the daily turn on. The most important of them are mentioned here.

- After turning on the pump laser, the TiSa won't run on full power and one has to adjust mirrors and perhaps even the etalon assembly to get the maximum output. The system should run for at least half an hour to let it thermalize before turning any knobs to improve the output power. The easiest way to bring it back to full power is by carefully tuning the mirrors guiding the pump beam to the TiSa. Most of the time this will be sufficient. If this does not work well enough the cover of the TiSa has to be lifted and screws of the upper and lower fold mirror have to be turned. If only small changes are done the direction of the output beam won't change, big corrections will result in some beam steering. The output coupler should never be touched because this will lead to a big change in the beam path of the output light. Minor beam steering can be easily corrected if one has two mirrors right at the output of the TiSa.

- If the laser intensity is showing big oscillations most probably the horizontal and vertical tilt of the thick etalon has to be adjusted. The thick etalon is very sensitive to temperature changes. If the temperature in the lab changed, it might be necessary to touch the "tilt adjust" screws for a full power output.

- If the wavelength of the laser can not be changed with the thick etalon knob most probably the piezo of the thick etalon broke. If this is the case the whole etalon has to be replaced because the piezo can't be changed easily.

- Sometimes it happens that the servo is oscillating which can be seen on the reference cavity display. Then one has to "relax" the servos by setting the lock knob to zero servo and then switch off the box for a few seconds. When the box is switched on again these oscillations are gone and the laser should work properly.

- Additional power enhancement can be achieved by adjusting the birefringent filter and the thin etalon so that all transmission peaks coincide.

Appendix B

Electronics

B.1 Laser servo system

In this appendix the electronic circuits used for locking the laser will be shown and explained. Each circuit was designed with the lowest necessary amplification, to get the maximal possible bandwidth.

B.1.1 PI controller

In Figure B.3 one can see the circuit for the HV and the piezo PI controller. The error signal is sent over a buffer amplifier, followed by a circuit to switch the sign of the feedback, a PID stage and an adder. Only the PI part of the controller is used but in principle it is capable of producing a derivative part as well. Figure B.1 shows the Bode plots of both controllers. In the HV part of the plots one can clearly see that the integrator is turning into a pure proportional amplifier below 100 Hz.
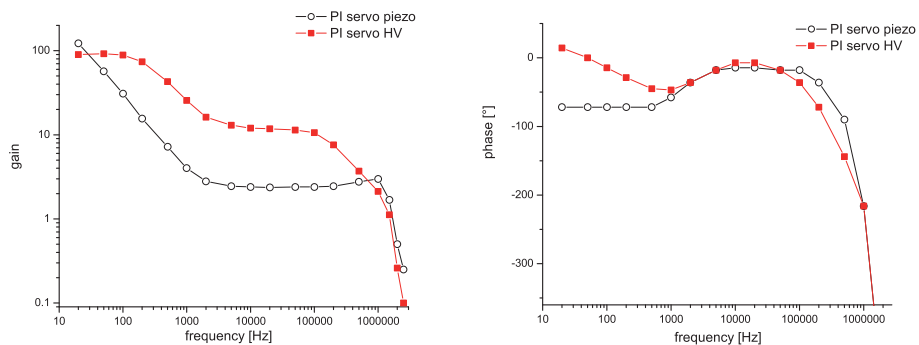

Figure B.1: Bode plot of the HV and the piezo PI stage

B.1.2 HV Amplifier

The circuit for the high voltage amplifier is shown in Figure B.4 where a buffer amplifier at the input is followed by the PA98 HV amplifier with a gain of roughly 30. The over all gain is adjusted with potentiometer ATTEN.1. The

circuit around the amplifier is designed such, that the bandwidth is maximal but without a big overshoot at the corner frequency. The Bode plot for the HV amplifier and the combination of HV amplifier and the PI servo is shown in Figure B.2.
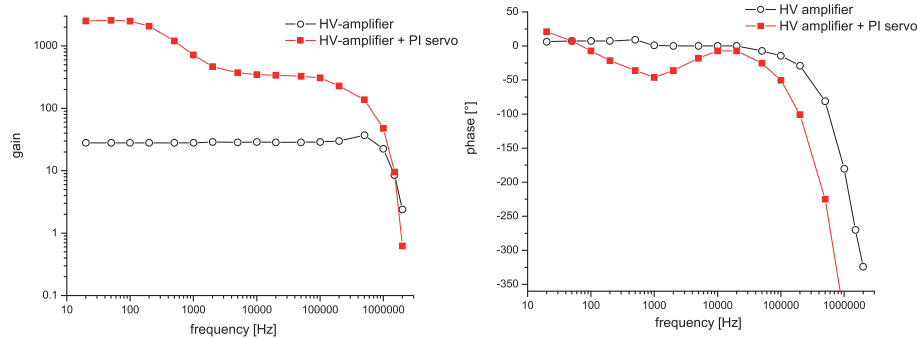

Figure B.2: Bode plot of HV amplifier and PI controller + HV amplifier

B.2 Fiber noise cancellation

The fiber noise cancellation (figure B.5) consists of a mixer comparing the photodiode signal with the reference. This DC signal is then low pass filtered and can be monitored at an output. The servo is a double PI stage where an additional offset is added. This offset can be tuned by R12 to bring the VCO near the required frequency so that the servo can lock. The VCO is protected by diodes against over-voltage. The circuit after the adding stage is a lock watch which disables the integrators for a certain time (determined by the timer NE555 with potentiometer R1) if the output value of the servo exceeds or falls below a threshold. The upper and lower thresholds can be set by the potentiometers R5 and R8. If the lock watch resets the integrators an acoustic signal is given by a speaker.

B.3 Additional electronics

Two phase-shifters have been built, the first one for the 2 kHz feedback inside the Coherent box (Figure B.6) and the second one (Figure B.7) for the generation of the local oscillator frequency for the PDH signal. In the 2 kHz shifter circuit one can see a buffer at the input followed by the circuit to switch the phase by 180°, then the phase shifter and a amplifier/attenuator circuit. The R-C combination at the output is taken from the circuit suggested in the Coherent manual.

The phase shifter for the PDH signal consists of a power splitter at the input, to split off the driving signal for the EOM. In the other channel follow two 180° phaseshifters a variable attenuator and an amplifier two generate the necessary phase and amplitude for the local oscillator signal.

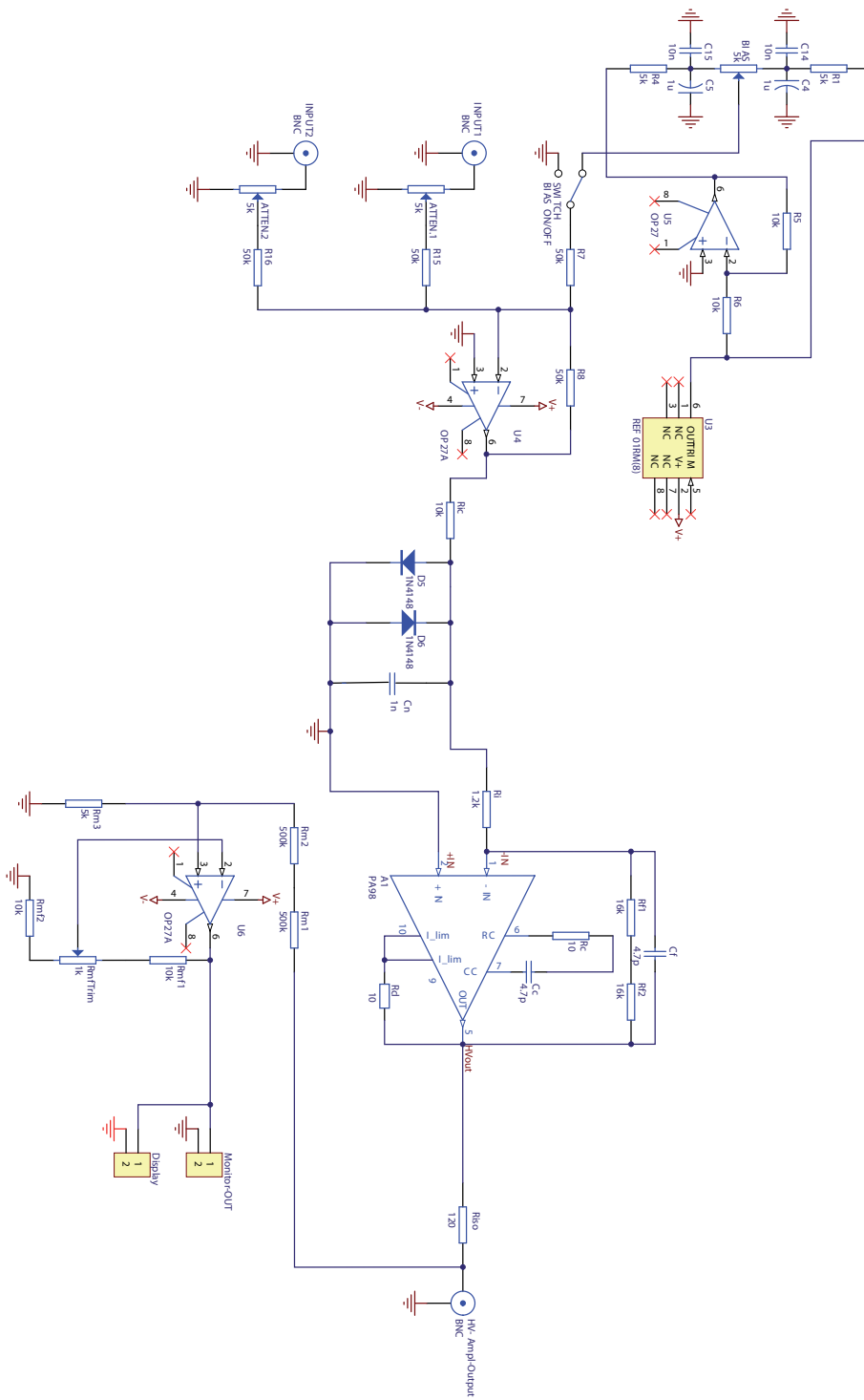Figure B.3: Circuit of the PI controller for HV and piezo part

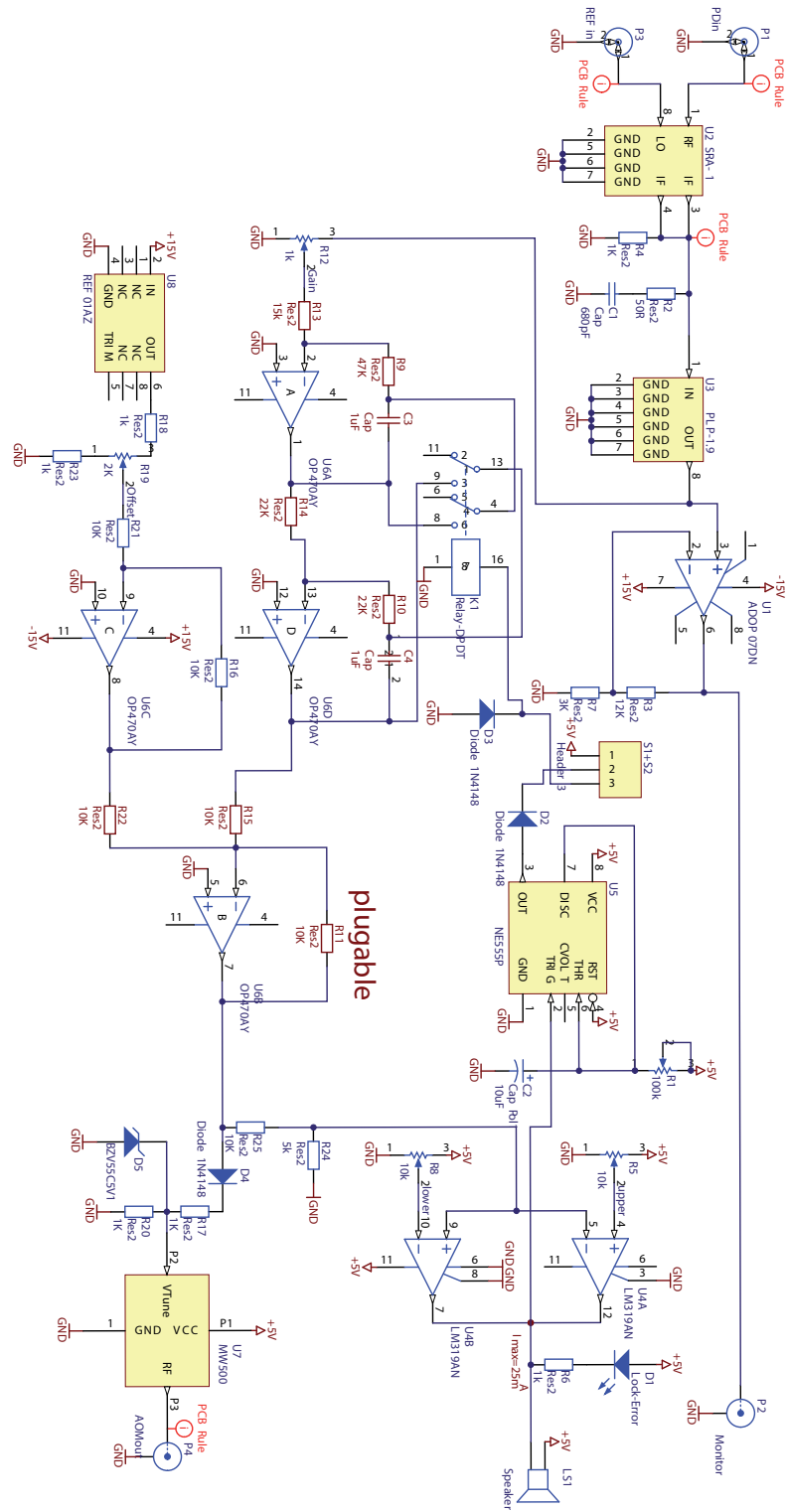Figure B.4: HV amplifier circuit
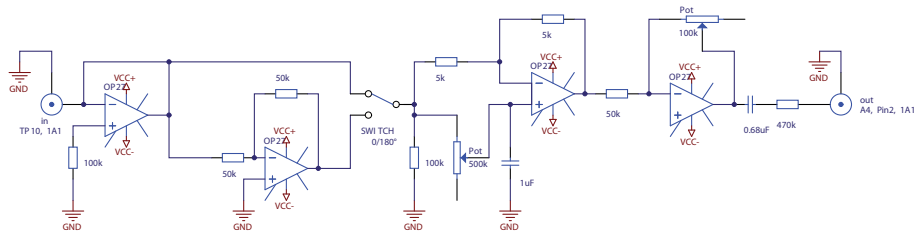
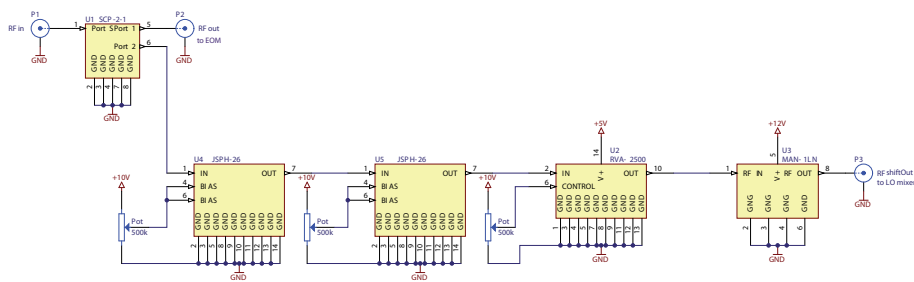Figure B.5: Fiber noise cancellation

Figure B.6: 2 kHz phaseshifter

Figure B.7: Phaseshifter for the PDH setup

Appendix C

Calculation of the true PDH peak to peak voltage

To get the true peak to peak voltage of the PDH signal one has to determine the voltage transfer function of the mixer. For that reason the dependence of the intermediate signal of the mixer on the RF input signal under the conditions of the lock setup has been measured. The measurement setup can be seen in Figure C.1.
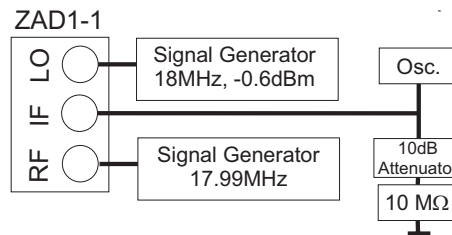

Figure C.1: Measurement setup for the ZAD1-1 transfer characteristics

The transfer characteristics of the mixer is shown in the Figure C.2

To calculate the real PDH signal the measured $480mV \pm 5mV$ is used to determine the necessary input voltage which is $1465mV \pm 170mV$. Then the corresponding output voltage was calculated that would have resulted from a linear mixer. The outcome was a PDH peak to peak voltage of $837mV \pm 96mV$. The fit to the data can be seen in Figure C.2.
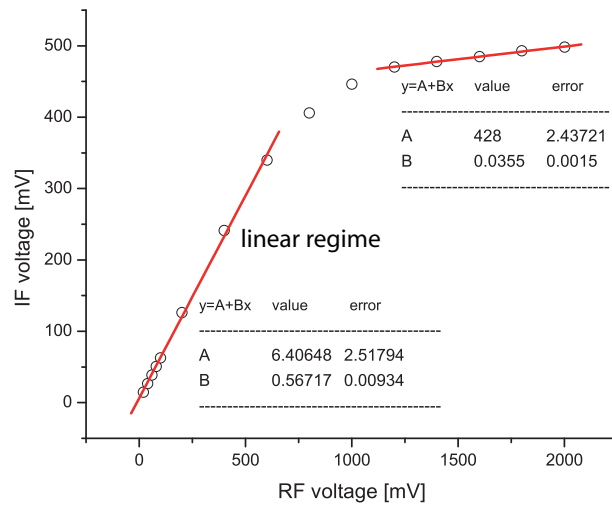
Figure C.2: Dependence of the IF signal of the ZAD1-1 mixer on the RF input signal (LO=-0.6 dBm)

Bibliography

[1]   H. Häffner, W. Hänsel, C. F. Roos, J. Benhelm, D. Chek-al-kar, M. Chwalla, T. Körber, U. D. Rapol, M. Riebe, P. O. Schmidt, C. Becher, O. Gühne, W. Dür, R. Blatt, *Scalable multiparticle entanglement of trapped ions*, Nature **438**, 643 (2005)

[2]   M. Riebe, H. Häffner, C. F. Roos, W. Hänsel, J. Benhelm, G. P. T. Lancaster, T. W. Körber, C. Becher, F. Schmidt-Kaler, D. F. V. James, R. Blatt, *Deterministic quantum teleportation with atoms*, Nature **429**, 734 (2004)

[3]   S. A. Diddams, Th. Udem, J. C. Berquist, E. A. Curtis, R. E. Drullinger, L. Hollberg, W. M. Itano, W. D. Lee, C. W. Oates, K. R. Vogel, D. J. Wineland, *An Optical Clock based on a Single Trapped $^{199}Hg^{+}Ion$*, Science Vol. **293**, 825 (2001)

[4]   B. C. Young, F. C. Cruz, W. M. Itano, J. C. Berquist, *Visible lasers with subhertz linewidths*, Phys. Rev. Letters **82**, 19 (1999)

[5]   Stephen A. Webster, Mark Oxborrow, Patrick Gill, *Subhertz-linewidth Nd:YAG laser*, Opt. Soc. **29**, 13 (2004)

[6]   Ch. Salomon, D. Hils, J. L. Hall, *Laser Stabilization at the milihertz level*, J. Opt. Soc. Am. B **5**, 8 (1988)

[7]   R. W. P. Drever, John L. Hall, F. V. Kowalski, *Laser Phase and Frequency Stabilization using an optical Resonator*, Appl. Phys. B **31**, 97 (1983)

[8]   D. Leibfried, E. Knill, S. Seidelin, J. Britton, R. B. Blakestad, J. Chiaverini, D. B. Hume, W. M. Itano, J. D. Jost, C. Langer, R. Ozeri, R. Reichle, D. J. Wineland, *Creation of a six-atom 'Schroedinger cat' state,* Nature **438**, 639 (2005)

[9]   J. Chiaverini, D. Leibried, T. Schaetz, M. D. Barrett, R. B. Blakestad, J. Britton, W.M. Itano, J.D. Jost, E. Knill, C. Langer, R. Ozeri, D.J. Wineland, *Realization of quantum error correction* Nature **432**, 602 (2004)

[10]   A. Wallraff, D. I. Schuster, A. Blais, L. Frunzio, R.- S. Huang, J. Majer, S. Kumar, S. M. Girvin, R. J. Schoelkopf, *Strong coupling*

of a single photon to a superconducting qubit using circuit quantum electrodynamics, Nature **431**, 162 (2004)

[11]   O. Mandel, M. Greiner, A. WIdera, T. Rom, T. W. Hänsch, I. Bloch *Controlled collisions for multi-particle entanglement of optically trapped atoms*, Nature **414**, 883 (2001)

[12]   Lieven M. K. Vandersypen, Matthias Steffen, Gregory Breyta, Costantino S. Yannoni, Mark H. Sherwood, Isaac L. Chuang, *NMR quantum computing: Realizing Shor's algorithm*, Nature **414**, 883 (2001)

[13]   D. P. DiVincenzo, *Two-bit gates are universal for quantum computation*, Phys. Rev. A **51**, 1015 (1995)

[14]   D. F. V. James, *Quantum dynamics of cold trapped ions with application to quantum computation*, Appl. Phys. B **66**, 181 (1998)

[15]   A. Steane, *The ion trap quantum information processor*, Appl. Phys. B **64**, 623 (1997)

[16]   J. I. Cirac, P. Zoller, *Quantum Computation with Cold Trapped Ions*, Phys. Rev. Lett. **74**, 20 (1995)

[17]   J. C. Bergquist, Randall G. Hulet, Wayne M. Itano, and D. J. Wineland, *Observation of Quantum Jumps in a Single Atom*, Phys. Rev. Lett. **57**, 1699 (1995)

[18]   Christian Roos, *Controlling the quantum state of trapped ions*, Dissertation (2000)

[19]   F. Kurth, T. Gudjons, B. Hilbert, T. Reisinger, G. Werth, A.-M. Martensson-Pendrill, *Doppler free "dark resonances" for hyperfine measurements and isotope shifts in Ca^+ isotopes in a Paul trap*, Z. Phys. D **34**, 227 (1995)

[20]   B. H. Rohde, *Experimente zur Quanteninformationsverarbeitung in einer linearen Falle*, Dissertation, (2001)

[21]   D. Leibfried, R. Blatt, C. Monroe, D. Wineland, *Quantum dynamics of single trapped ions*, Rev. Mod. Phys. **75**, 1 (2003)

[22]   J. Eichler, H. J. Eichler, *Laser*, Bauformen, Strahlführung, Anwendungen, 5. Auflage, Springer (2003)

[23]   Coherent, *Service manual*, 699 ring dye laser

[24]   W. Demtröder, *Laser Spectroscopy*, Basic concepts and Instrumentation, Third Edition, Springer (2003)

[25]   A. E. Siegman, *Lasers*, University Science Books 1986

[26]   Schaefter & Kirchhoff, *Grundlagen zu Faserkol-limatoren 60-FC*, Manual zu Faserkollimatoren, $http://www.sukhamburg.de/download/fk60fc_d.pdf$

[27]   M. Houssin, M. Jardino, M. Desaintfuscien, *Comparison of the calculated transient response of a Fabry-Perot used in reflection and in transmission*, Rev. Sci. Inst. **61**, 11 (1990)

[28]   Mark Notcutt, Long-Sheng Ma, Jun Ye, John L. Hall, *Simple and compact 1-Hz laser system via improved mounting configuration of reference cavity*, Optics Letters **30**, 14 (2005)

[29]   H. Rohde, J. Eschner, F. Schmidt-Kaler, R. Blatt, *Optical decay from a Fabry-Perot cavity faster than the decay time*, J. Opt. Soc. Am. B **19**, 1425 (2002)

[30]   M. J. Lawrence, B. Willke, M. E. Husman, E. K. Gustavson, R. L. Byer, *Dynamic response of a Fabry-Perot Interferometer*, J. Opt. Soc. Am. B **16**, 523 (1999)

[31]   Discussion with J. Alnis at ICAP 2006 in Innsbruck

[32]   Long Sheng Ma, Peter Jungner, Jun Ye, John L. Hall, *Delivering the same optical frequency at two places: accurate cancellation of phase noise introduced by an optical fiber over the time-varying path*, Optics Letters **19**, No. 21 (1994)

[33]   John L. Hall, Matthew S. Taubman, Jun Ye, *Laser Stabilization*, Handbook of optics IV, 2nd edition, 2001 McGraw Hill

[34]   Willhelm Haager, *Regelungstechnik*, Verlag Hoelder-Pichler-Tempsky, 2 Auflage, (1997)

[35]   John Bechhoefer, *Feedback for physicists: A tutorial essay on control*, J. Opt. Soc. Am. B **16**, 523 (1999)

[36]   T. W. Hänsch, B.Couillaud, *Laser frequency stabilization by polarization spectroscopy of a reflecting reference cavity*, Opt. Commun. **35**, 3 (1980)

[37]   R. L. Barger, M. S. Sorem, J. L. Hall, *Frequency stabilization of a cw dye laser*, Appl. Phys. Letters **22**, 573 (1973)

[38]   Eric Black, *Notes on the Pound Drever Hall technique*, Technical Note of the LIGO Project, (1998)

[39]   Eric D. Black, *An introduction to Pound Drever Hall frequency stabilization*, Am. J. Phys. **69**, 1 (2001)

[40]   Edward A. Whittaker, Manfred Gehrtz, Gary C. Bjorklund, *Residual amplitude modulation in laser electro-optic phase modulation*, J. Opt. Soc. Am. B **2**, 8 (1985)

[41]   D. S. Elliott, Rajarshi Roy, S. J. Smith, *Extracavity laser band-shape and bandwidth modification*, Phys. Rev. A **26**, 1 (1982)

[42]   Mandel and Wolf, *Optical coherence and quantum optics*, Cambridge University Press (1995)

Danksagung

Das Gelingen dieser Arbeit wäre ohne die Hilfe und Geduld Vieler nicht möglich gewesen. Ihnen allen möchte ich hiermit meinen Dank aussprechen.

An erster Stelle Prof. Rainer Blatt, der es mir ermöglicht hat, meine Diplomarbeit in einem interessanten Umfeld zu machen.

Der ganzen Gruppe die ein Klima geschaffen hat, in dem ich gerne arbeite. Besonders aber:

- Der Kochgruppe für das gute Essen und die gute Gesellschaft in den Mittagspausen.

- Mike für seine tatkräftig Hilfe an der "real laser" Front.

- Jan für die tägliche Unterstützung und die Diskussionen im Labor.

- Christian Roos für ein offenes Ohr für Fragen und besonders für das Korrekturlesen meiner Arbeit.

Nicht zu vergessen sind meine Freunde. Durch sie ist mein Leben auch ausserhalb des Labors immer interessant und lustig.

Ein "Danke" gilt auch meinen Eltern, die mir dieses Studium erst ermöglicht haben.

Meiner Freundin Astrid gebührt ein besonderer Dank für das Verständnis und die Unterstützung in allen Lebenslagen.